AZƏRBAYCAN MİLLİ ELMLƏR AKADEMİYASI

AZƏRBAYCAN ASTRONOMİYA JURNALI

2017, Cild 12, № 1

AZERBAIJAN NATIONAL ACADEMY OF SCIENCES

ASTRONOMICAL JOURNAL OF AZERBAIJAN

2017, Vol. 12, No. 1

Bakı-2017 / Baku-2017

ASTRONOMICAL JOURNAL OF AZERBAIJAN

Founded in 2006 by the Azerbaijan National Academy of Sciences (ANAS)
Published in the Shamakhy Astrophysical Observatory (ShAO) named after N. Tusi, ANAS
ISSN: 2078-4163 (Print), 2078-4171 (Online)

Editorial board

Editorial Office address:	ANAS, 30, Istiglaliyyat Street, Baku, AZ-1001, the Republic of Azerbaijan
Address for letters:	ShAO, P.O.Box №153, Central Post Office, Baku, AZ-1000, Azerbaijan
E-mail:	aaj@shao.az
Phone:	(+994 12) 510 82 91
Fax:	(+994 12) 497 52 68
Online version:	http://www.aaj.shao.az

ASTRONOMICAL JOURNAL OF AZERBAIJAN

2017, Vol. 12, № 1

Contents

ShaFES: SHAMAKHY FIBRE ECHELLE SPECTROGRAPH

Kh. M. Mikailov [a*], ***F. A. Musayev*** [b], ***I. A. Alakbarov*** [a], ***B. N. Rustamov*** [a], ***O. V. Khalilov*** [a]

[a] *Shamakhy Astrophysical Observatory named after N.Tusi, Azerbaijan National Academy of Sciences, Shamakhy region, Azerbaijan*

[b] *Special Astrophysical Observatory, Russian Academy of Sciences, Nizhnij Arkhyz, Russia*

The paper describes the high-resolution fiber-optic echelle spectrograph developed for the Cassegrain focus of the 2-m telescope at the Shamakhy Astrophysical Observatory. The schematic optical circuit and circuit of a suspended part of the spectrograph are presented. Spectrograph operates in two modes with spectral resolutions of 28000 and 56000, in $\lambda\lambda 3700 - 8500$ ÅÅ region of wavelengths. Results of testing of positional and photometric performances of the spectrograph are analyzed.

Keywords: Instrumentation – Spectrographs

1. INTRODUCTION

Among various analysis methods of the radiation coming from space the method of spectroscopic researches using the decomposition principle of incoming radiation to the components on wavelengths (frequencies) holds a peculiar place. Different spectral instruments which allow studying the spectra of absorption, radiation, reflection, scattering, etc. are used for this purpose. The study of spectra gives the most complete information about both the physical processes occuring in a radiation source and the properties of the environment through which this radiation propagates.

Greater possibilities have been provided for spectral observations from the date of exploitation of the 2-m telescope at the Shamakhy Astrophysical Observatory (ShAO). The telescope is equipped with spectrographs with different resolution

* E-mail: mikailov.kh@gmail.com

powers. Photoplates of different foreign firms were used as a light detector. However the suspension of a production of such light detectors and creation of highly sensitive multi-channel light detectors of CCD arrays (CCD-Charge Coupled Device), led to broad application in astrophysical researches of echelle spectrographs. Echelle spectrographs with CCD cameras, allow eliminating the creation of large-size spectrographs and fix the problem of obtaining a high resolution.

In 1993 the echelle spectrometer (R=30000) was built using optical components and units of the classical spectrograph for coude focus of the 2-m telescope at the ShAO [1,2].

In 2003 considering the subject of ShAO on which the objects of $8^m - 11^m$ stellar magnitude are mainly investigated, the suspended echelle-spectrograph was built on the basis of the spectrograph UAGS for Cassegrain focus of the 2-m telescope to broaden variety of astronomical problems of astrospectroscopy and to obtain a qualitative spectral material of weaker objects [3].

When measuring integral intensity of the line - equivalent width - small variations of a line form related to the unstable star position in a spectrograph slit – are inessential. Therefore suspended spectrographs are used even today.

Equipment of telescopes with high resolution spectrographs is very important for solution of the modern astrophysical problems, as well as for participation in international projects. One of the advanced methods of increasing the characteristics of a spectrograph is to develop and apply specialized spectrographs with a fiber-optic input in astronomy. Creation process of the first tool of this kind is described in [4]. Now several tens of high resolution spectrographs in which light is transferred through the fiber-optical channel have been built [5,7–9]. Such way of transferring light energy has a number of obvious advantages. In other words, the placement of the spectrograph outside the moving parts of the telescope design, provides it with a higher mechanical and temperature stability and, consequently, higher than traditional slit spectrographs, the accuracy of position spectroscopic measurements (that is, in particular, important in measuring radial velocity of stars). Thanks to a high mechanical stability, on fiber-optical spectrographs the accuracy of measuring radial velocity of stars was reached up to 1 m/s and higher [9]. Establishment of the first tools of this kind permits to begin a number of new unique researches the performance of which was difficult or even impossible by using traditional circuits of spectrographs.

Some instruments, including CCD camera cooled by liquid nitrogen with (size) a matrix of $4K \times 4K$ elements were purchased within the modernization program of the observational technique in the ShAO. Due to a large overall dimension of CCD camera, it can be used only in stationary spectrographs. A fiber-optic echelle - spectrograph for Cassegrain focus of the 2-m telescope at the ShAO (ShaFES-Shamakhy Fibre Echelle Spectrograph) is being built since 2015. The

spectrograph consists of two main units: a massive stationary part (Fig. 1) and relatively light suspended part (Fig. 2), fixed in Cassegrain focus of the telescope. The units are linked to each other with optical fiber 200 microns in diameter and 20 m in length.

2. STATIONARY PART OF THE SPECTROGRAPH

Stationary part of the instrument was constructed using the autocollimating diagram and provides spectral resolution R=56000 in the range of wavelengths $\lambda\lambda$3800–8500 ÅÅ.

Fig. 1 shows the optical diagram of a stationary part of the fiber-optic echelle - spectrograph for Cassegrain focus of the 2-m telescope at the ShAO.

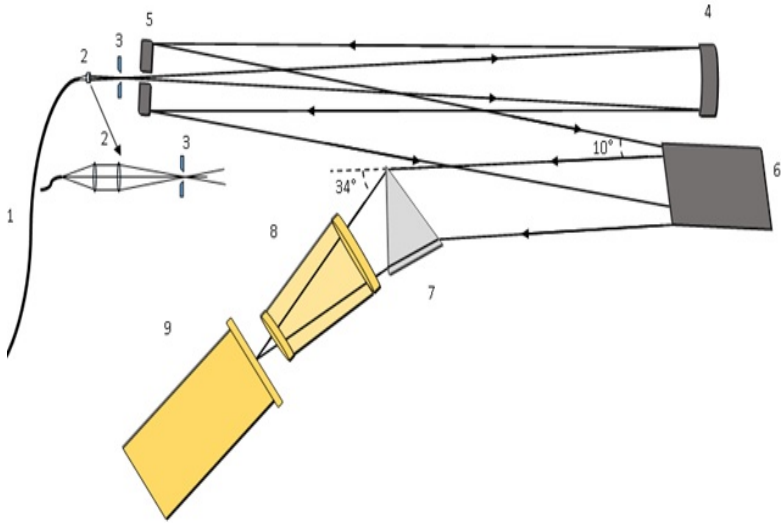

Fig. 1. The optical layout of the statonary part of the spectrograph. 1-optical fiber d=200 mkm in diameter, 20 m in length, 2- group of microlenses, 3-entrance slit, 4-collimator, 5- plane mirror with hole of 10 mm, 6- echelle grating, 7-cross-disperser prism, 8-objective Canon, 9-detector-CCD camera.

Stationary part of the spectrograph is located in the isolated room under the dome and provided with the thermostat. Protective cover of the spectrograph is well isolated and the access to the optical-mechanical components is provided with one person. This guarantees the stable temperature of the spectrograph. Basic elements of the echelle-spectrograph are located in the stationary part: mechanical component retaining an optical fiber with coordinating optics at an output face (microlens), collimator, echelle grating, element with crossed dispersion (prism), lens objective and radiation detector (CCD camera).

All optical elements are mounted on the iron alloy table. Components of all optical details are supplied with the adjusted devices used only in primary installation of the spectrograph. The table is fixed on a steel channel frame with adjustable supports to increase stiffness.

The image of the object under study is transferred to the slit (3) with optical fibers (1), 200 mkm core diameter, numerical aperture of N=0.25. For coordination (filling) with collimator (4) the lenses (2) with light-gathering power of 1:10 were inserted on the output of the optical fiber. Focal distance of the collimator is 1000 mm, diameter of the collimated beam is 100 mm. Using a plane mirror (5) (d=110 mm) the collimated beam falls on a surface of the echelle grating (6) - the basic dispersive element and a vertical dispersion of a light occurs. The size of the grooved region is $200 \times 300\ mm^2$, the groove density is 37.5 gr/mm , the blaze angle is 64°. For operation in autocollimating mode echelle grating was installed at the angle of 26° to the horizontal plane. It was oriented down to prevent the dust from falling on the surface.

A heavy flint prism with apex angle of 45° was used as a cross-disperser (7). Horizontal light dispersion occurs in it to divide echelle orders. Refraction index for red region in a glass is equal to 1,6444 and for violet region - 1,6852. The prism operates in the deviation minimum mode, The prism works in the mode of minimum deviation, for the central wavelength it is $\sim 34°$.

F/2.8 lens objective Canon with an effective focus of 400 mm is used as a focusing camera (8).

3. SUSPENDED PART OF THE SPECTROGRAPH

Functional suspended part contains: optics matching an image scale of a star with sizes of optical fiber, calibration node with sources of a line and continuous spectrum, monitoring means for the location of an object at the fiber inlet (detect). Fig. 2 shows the diagram of suspended (pre-fiber-optic) part of the spectrograph which was placed in Cassegrain focus of the 2-m telescope at the ShAO. Moving mirror (5) for calibration lamps of line and continuous spectra, system of positioning optic fiber and guiding detector (10) were inserted in suspended part of the device. Telescope produces an image on focal plane - F1, where the input aperture is located (1). Ratio aperture of Cassegrain focus of the 2-m telescope equals to F/14.5. We have the possibility of using two gears. Beam from the 2-m mirror by the gears of focus (12) with ratio aperture F/9 or F/6 is collimated for focal plane with a group of lenses (2) and then converted to the same aperture with a group of lenses (3) on focal plane – F2, where the inlet head of fiber is located. The size of the input aperture made of reflecting plate, is 200 microns that conforms to 3.5 angular seconds. Considering that the image generally makes

at least 3 angular seconds we selected ratio aperture F/6. The image of the star under study fails to optical fiber through aperture, the reflection from the edges of an aperture by a plane mirror (8) and focusing lens (9) gets to the revision camera of a field (10) the objective of which is also focused on a front surface of an aperture plate. The image from the revision camera of a field is transferred to the monitor (11) which is in the observational room. Guiding is performed there.

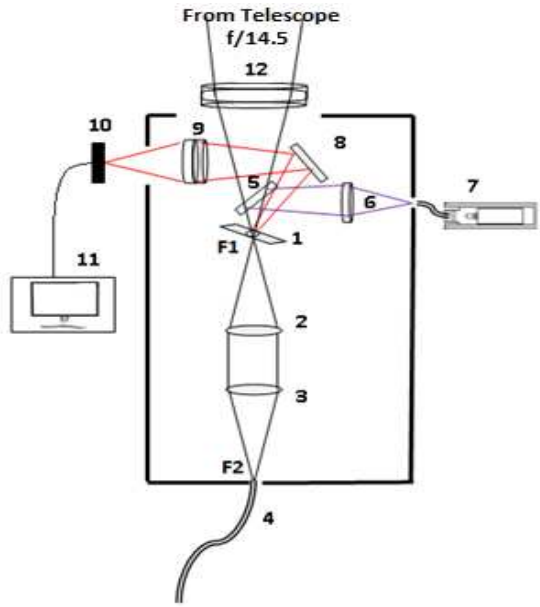

Fig. 2. The optical layout of the suspended part of the spectrograph. 1-entrance aperture-telescope focal plane; 2- collimating lenses, 3- focusing lenses; 4-optical fiber; 5-moving diagonal mirror; 6- group of lenses; 7- calibration lamps; 8-diagonal mirror; 9- guiding detector lens; 10-guiding detector; 11-monitor; 12 –aperture reductor.

Artificial light sources (7) for calibration on wavelengths (lamp with the hollow thorium cathode filled with a mixture of gases) and for a plane field (a halogen lamp) are placed in Cassegrain focus. Light beam from a source using the lenses (6) is focused and directed by a mirror (5) to an input aperture. Box of calibrating lamps is connected to a suspended part with a short optical fiber. Box of a suspended part of the spectrograph has the sizes of $50 \times 50 \times 100$ mm and about 1 kg mass.

4. CCD CAMERA

CCD camera manufactured in the USA with $4K \times 4K$ pixels cooled by liquid nitrogen with element size of 15 microns is used as a light receiver. The cam-

era cools CCD-chip till the temperature (programmed by selection) at a range of $-110°$C to $-145°$C, and holds it with the accuracy of +/-0,1°C. Recommended temperature of CCD-chip under the conditions of real observations is $-120°C$. Cooling system has a capacity of 3 litre and operability time between fillings with nitrogen not less than 24 hours. CCD STA4150A (serial number 16314) of semiconductive technology **Associates, Inc.** has an anti-reflective coating, which allows maximizing its quantum efficiency in the wavelength range of $\lambda\lambda$3000-9000 ÅÅ.

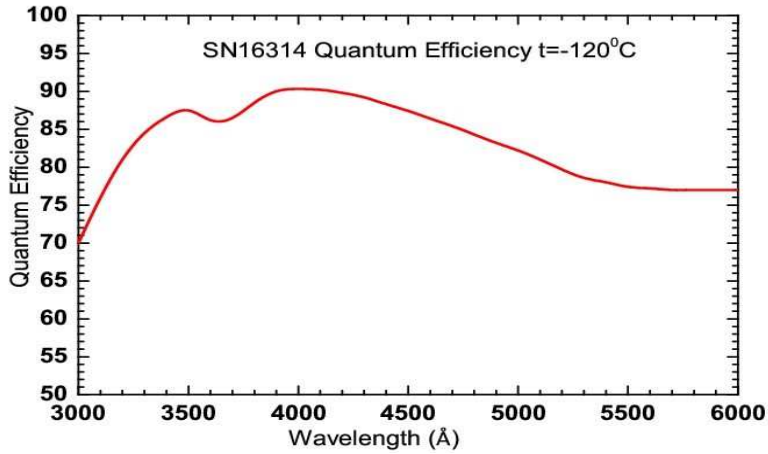

Fig. 3. Curve of quantum efficiency of CCD camera: model STA4150A, serial number SN 16314.

Fig. 3 shows the curve of quantum efficiency of CCD camera. Quantum efficiency in wavelength range of $\lambda\lambda 3000-6000$ ÅÅ is higher than 70%. In the range of $\lambda\lambda$6000-8000 ÅÅ it is not lower than 70% according to the technical instruction of this firm. Our device has a distinctive feature - efficiency in UV range. At λ 4000 Å quantum efficiency reaches 90%. Parameters of CCD camera are: number of pixels 4096×4096; pixel size 15x15mkm; size of photosensitive area $61,44 \times 61,44mm$; operating spectral range $\lambda\lambda$3000-9000 ÅÅ. Full frame reading time for three modes: FST-fast-6.5 sec, MED-average-19 sec, SLW-slow-40.7 sec. In the SLW mode, gain = 1.27 e-/ADU, Read Out Noise (RON) = 3.74 electrons. In MED mode, gain = 2.24 e-/ADU, RON = 4.8. In the FST mode, gain = 2.0 e-/ADU, RON = 7.5. Measured dark current makes 4e-/pixel/hou. Control and data transfer to the computer is carried out on a fiber optic cable 15 m in length.

5. OPTICAL PARAMETERS OF ECHELLE SPECTRUM

As it is known general form of the diffraction equation appears as follows

$$\sin\varphi + \sin\varphi^{'} = Nk\lambda_k \tag{1}$$

Where φ - angle of incidence on a grating of a parallel optical beam, i.e. an angle which forms rays with a normal of grating. $\varphi^{'}$ - diffraction angle, N=1/d – density of grating grooves, d – grating period, k – spectral order, λ_k central wavelength of a spectrum on given order. If the grating operates in autocollimation mode, ($\varphi = \varphi^{'} = \gamma$), the equation of diffraction takes the form:

$$2\sin\gamma = Nk\lambda_k \tag{2}$$

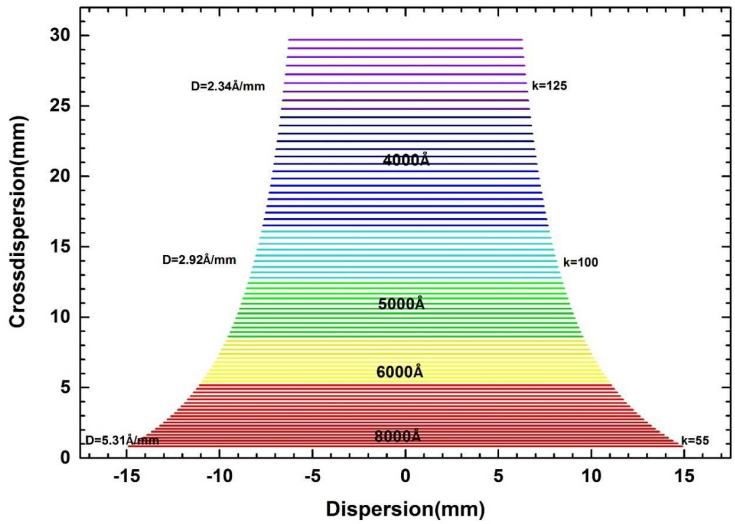

Fig. 4. Output format of Shamakhy Fiber echelle-spectrograph-ShaFES, Echelle: 37.5 grooves/mm, Blaze angle 64°, σ = 10°. heavy flint prism with apex angle of 45°. Camera with effective focus of 400 mm.

γ – blaze angle. To direct the beam dispersed from echelle grating to cross-disperser, the main cross-section of echelle grating forms small angles ($\delta = 10°$) with collimator axis. In this case the diffraction equation takes the following form [10]

$$2\sin\gamma = k\lambda_k N/\cos\delta \tag{3}$$

The images of a slit (spectral lines) turn out to be non-perpendicular to the dispersion that leads to losses of resolving power of the spectrograph.

To eliminate the inclination of spectral lines the slit was turned around a collimator axis through an angle of tgε =2 tgγ tgδ. Knowing that $\delta = 10°$ and $\gamma = 64°$ we will receive for $\varepsilon = 36°$.

Considering the equation (3), the key optical parameters of the echelle spectrum obtained in focal plane of the camera of the echelle spectrograph were calculated (Fig. 4; Table 1).

Table 1. Parameters of echelle spectrum

k	λ_{min}(Å)	λ_{cen}(Å)	λ_{max}Å	$\delta\lambda$Å	D_k(Å/mm)	k	λ_{min}(Å)	λ_{cen}(Å)	λ_{max}Å	$\delta\lambda$Å	D_k(Å/mm)
55.00	8505.884	8583.16	8661.91	156.07	5.31	91.00	5159.28	5187.63	5216.29	57.01	3.21
56.00	8355.29	8429.89	8505.84	150.55	5.22	92.00	5103.50	5131.24	5159.28	55.78	3.18
57.00	8209.98	8282.00	8355.29	145.31	5.13	93.00	5048.92	5076.06	5103.50	54.58	3.14
58.00	8069.64	8139.21	8209.98	140.34	5.04	94.00	4995.49	5022.06	5048.92	53.43	3.11
59.00	7934.02	8001.25	8069.64	135.62	4.95	95.00	4943.18	4969.20	4995.49	52.31	3.08
60.00	7802.88	7867.90	7934.02	131.14	4.87	96.00	4891.98	4917.44	4943.18	51.22	3.04
61.00	7676.00	7738.92	7802.88	126.88	4.79	97.00	4841.78	4866.74	4891.96	50.17	3.01
62.00	7553.18	7614.10	7676.00	122.82	4.71	98.00	4792.63	4817.08	4841.78	49.16	2.98
63.00	7434.24	7493.24	7553.18	118.95	4.64	99.00	4744.46	4768.42	4792.63	48.17	2.95
64.00	7318.98	7376.16	7434.24	115.26	4.57	100.00	4697.25	4720.74	4744.46	47.21	2.92
65.00	7207.24	7262.68	7318.98	111.74	4.50	101.00	4650.97	4674.00	4697.25	46.28	2.89
66.00	7098.86	7152.64	7207.24	108.38	4.43	102.00	4605.60	4628.18	4650.97	45.38	2.87
67.00	6993.69	7045.88	7098.86	105.17	4.36	103.00	4561.10	4583.24	4605.60	44.50	2.84
68.00	6891.59	6942.26	6993.69	102.10	4.30	104.00	4517.45	4539.17	4561.10	43.65	2.81
69.00	6792.43	6841.65	6891.59	99.16	4.24	105.00	4474.63	4495.94	4517.45	42.82	2.78
70.00	6696.08	6743.91	6792.43	96.35	4.17	106.00	4432.62	4453.53	4474.63	42.02	2.76
71.00	6602.43	6648.93	6696.08	93.65	4.12	107.00	4391.39	4411.91	4432.62	41.23	2.73
72.00	6511.36	6556.58	6602.43	91.07	4.06	108.00	4350.91	4371.06	4391.39	40.47	2.71
73.00	6422.77	6466.77	6511.36	88.59	4.00	109.00	4311.18	4330.95	4350.91	39.73	2.68
74.00	6336.56	6379.38	6422.77	86.21	3.95	110.00	4272.16	4291.58	4311.18	39.02	2.66
75.00	6252.64	6294.32	6336.56	83.93	3.90	111.00	4233.85	4252.92	4272.16	38.32	2.63
76.00	6170.90	6211.50	6252.64	81.73	3.85	112.00	4196.21	4214.95	4233.85	37.63	2.61

Continuation of the table 1

k	λ_{min}(Å)	λ_{cen}(Å)	λ_{max}Å	$\delta\lambda$Å	D_k(Å/mm)	k	λ_{min}(Å)	λ_{cen}(Å)	λ_{max}Å	$\delta\lambda$Å	D_k(Å/mm)
77.00	6091.28	6130.83	6170.90	79.62	3.80	113.00	4159.24	4177.65	4196.21	36.97	2.59
78.00	6013.68	6052.23	6091.28	77.60	3.75	114.00	4122.92	4141.00	4159.24	36.33	2.56
79.00	5938.04	5975.62	6013.68	75.64	3.70	115.00	4087.22	4104.99	4122.92	35.70	2.54
80.00	5864.27	5900.92	5938.04	73.76	3.65	116.00	4052.14	4069.60	4087.22	35.08	2.52
81.00	5792.32	5828.07	5864.27	71.95	3.61	117.00	4017.65	4034.82	4052.14	34.49	2.50
82.00	5722.11	5757.00	5792.32	70.21	3.56	118.00	3983.75	4000.63	4017.65	33.90	2.48
83.00	5653.58	5687.64	5722.11	68.53	3.52	119.00	3950.41	3967.01	3983.75	33.34	2.46
84.00	5586.67	5619.93	5653.58	66.91	3.48	120.00	3917.63	3933.95	3950.41	32.78	2.44
85.00	5521.33	5553.81	5586.67	65.34	3.44	121.00	3885.38	3901.44	3917.63	32.24	2.42
86.00	5457.50	5489.23	5521.33	63.83	3.40	122.00	3853.66	3869.46	3885.38	31.72	2.40
87.00	5395.13	5426.14	5457.50	62.37	3.36	123.00	3822.46	3838.00	3853.66	31.20	2.38
88.00	5334.17	5364.48	5395.13	60.96	3.32	124.00	3791.76	3807.05	3822.46	30.70	2.36
89.00	5274.57	5304.20	5334.17	59.60	3.28	125.00	3761.55	3776.59	3791.76	30.21	2.34
90.00	5216.29	5245.27	5274.57	58.28	3.25	126.00	3731.81	3746.62	3761.55	29.74	2.32

6. RESOLVING POWER OF ECHELLE SPECTROGRAPH

Real resolving power of echelle spectrograph, as well as classical spectrographs, is defined by the formula the smallest interval of wavelength corresponding to resolution of the light detector also expresses as follows: Real resolving power of echelle spectrograph, as well as classical spectrographs, is defined by the formula $R = \lambda_k/\Delta\lambda_k$. $\Delta\lambda_k$ - the smallest interval of wavelength conforming to the resolution of the light detector is expressed as

$$\Delta\lambda_k = b^{'} D_k = \frac{cos\varphi^{'}}{Nkf_{cam}}$$

$\Delta\lambda_k$ - spectral resolution. D_k–reverse linear dispersion, $b^{'}$- width of the slit image in the focal plane of the camera. In modern CCD array type light detectors, as well as on photoplates, the image of slit width conforms to the sizes of 2 sensitive elements ($b^{'} = 2pix$). Width of the slit is defined by the resolution of the light detector and is expressed as $b = f_{col}\ b^{'}/f_{cam} \cdot f_{col}, f_{cam}$ – focal distance

of the collimator and camera, respectively. Thus, real resolving power determined by the resolution of a light detector

$$R = \frac{\lambda_k}{\Delta\lambda_k} = \frac{2f_{cam}tg\gamma}{b'}$$

Thus, the resolving power of the echelle spectrograph depends on blazing angle of the echelle grating, on parameters of optical system and the sizes of sensitive elements of the light detector.

In our case f_{cam} = 400 mm, $\gamma = 64°$, b' = 30 mkm and, therefore, we get: R=56000. The distances between orders allow the spectrograph to operate in two modes. 1 pix=15 mkm R=56000 and 1pix=30 mkm R=28000. Change of spectral resolution occurs programmatically, by transition when reading a frame from binning 1 to binning 2, but reduction of spectral resolution is a compulsory measure to achieve as much relation signal/noise as possible while observing weak stars with small flux even for the 2-m telescope. In the course of observations OWL program allows moving from one mode to another in a short period. It is possible to obtain spectra of stars with 8 and 10 stellar magnitudes, with relation signal/noise (S/N) = 150-200, at λ = 5800Å for hour exposure with resolution of R=56000 and R=28000, respectively.

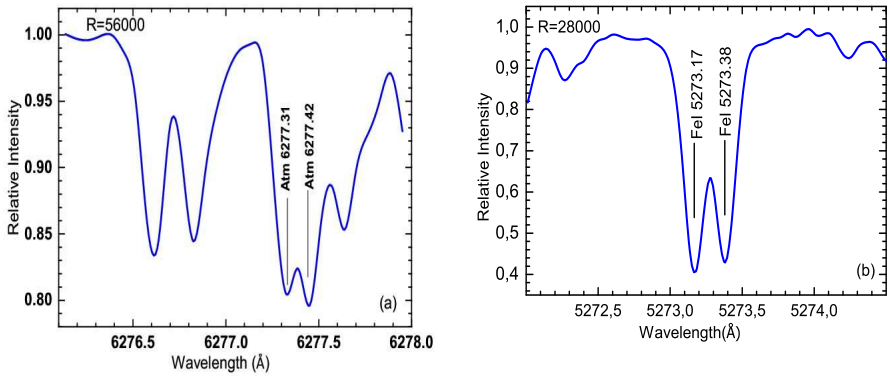

Fig. 5. Spectral region of a star (a)- α Cyg and (b)-Sky, showing resolving power of the spectrograph.

7. OBTAINING SPECTRA

Control of a CCD matrix – exposure time of spectra, monitoring the temperature of the chip, reversal of echelle spectrum, selection of a chip format conforming

to the format of echelle spectrum are performed using "Owl 3.01" license program [11]. For resolving power of R=56000 format of the chip 2400 pixels were selected in the direction of dispersion, but in the direction of cross-dispersion 1650 pixels. For resolving power of R=28000 format of the chip 1250 pixels were selected in the direction of dispersion, but in the direction of cross-dispersion 860 pixels. Files with spectra must have the extension of *.fit or *.fts. Layout of echelle orders in frames is horizontal. That is to say the direction of dispersion is horizontal, but the direction of cross-dispersion is vertical. Wavelenght increases from top to down and from left to right. It excludes excess procedures in reduction of a spectrum. All frames must be produced in identical value of a conversion factor (gain) of CCD camera. Intensity of a plane field and thorium - argon lamp must be sufficiently high, but it must not exceed the linearity limits of CCD (about 65 000 for gain=0.54, and 40 000 for gain=2.17).

8. REQUIREMENTS TO PROCESSED FRAMES

Spectra are processed using the new version of the program DECH [12]. To perform the processing besides spectra of the object it is necessary to produce a full set of calibration frames: dark (or bias), flat-field, ThAr or Sky. CCD matrix is cooled to very low temperatures about $-140°C$ to reduce the impact of a thermal noise. At such cooling degree of CCD array thermal electrons are practically absent and, as a result, dark frame doesn't differ from a bias frame even at exposures in tens of minutes. Therefore, in this case there is no sense in wasting observation time for getting dark frames.

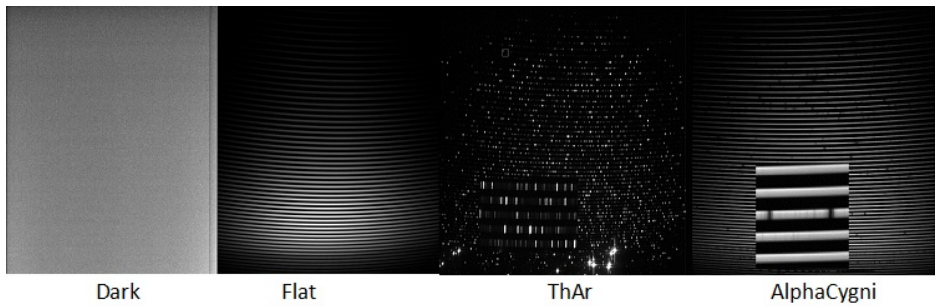

Fig. 6. Fragments of various type images.

Flat- image of a spectrum of a lamp of a plane field. The lamp of a plane field has a continuous smooth spectrum. Sensitivity of pixels in a matrix isn't identical, spectrum of a plane field is obtained to consider heterogeneity of sensitivity of different pixels and fringe (fringe - interferential bands arising in a red part of

spectrum). Lamps were used as light sources to produce the image of plane fields: Halogen lamps in red and Led lamps in blue spectral region. Spectra of lamps can be obtained both simultaneously and separately. In energy distribution peaks are in the range of wavelengths λ5600 Å and λ4400 Å, Halogen and Led lamps, respectively (see Fig. 7).

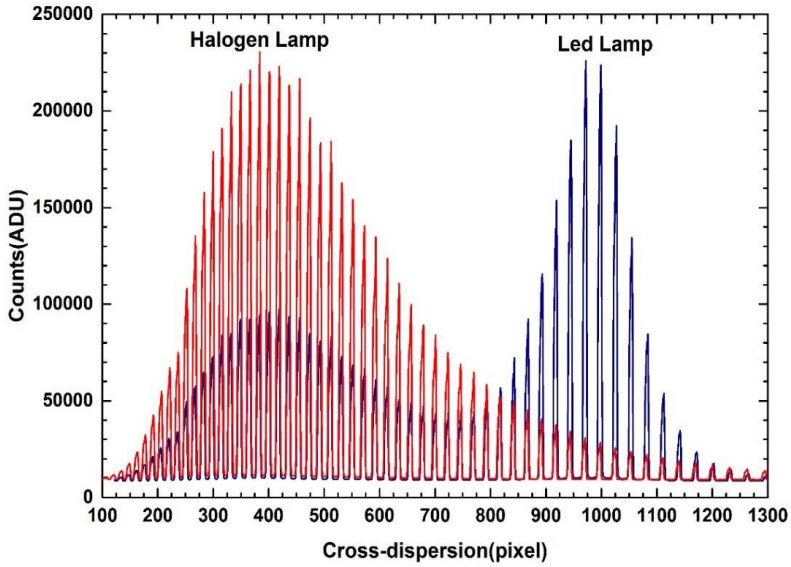

Fig. 7. Light distribution on spectral orders of halogen (left) and LED (right) lamps. Maximum intensity for halogen lamps conforms to $\lambda\lambda$6000-5000 ÅÅ, and for LED lamps about λ 4400 Å.

Comparison spectrum serves for the colibration of a spectrum of the object to wavelengths. We must say that observational materials are obtained in the system of coordinates of CCD array. We should move to a space of wavelengths or at least, each element of a receiver should assign relevant wavelength. Comparison spectrum must contain many narrow lines distributed equally throughout the spectrum which has a constant wavelength. Thorium - argon (ThAr) lamps are usually used for wavelength colibration. Morning or evening twilight spectrum, in fact, sunlight spectrum scattered by atmosphere is used for this purpose. It has a form of a common G star spectrum with narrow absorption lines of the Sun and earth atmosphere.

At a resolution of R = 56000 the width of emission-spectral lines of ThAr-lamp is limited by the spectral resolution of ShaFES device, and all spectral range from near UV to near IR is almost evenly filled with emission lines. For example, Fig. 8a shows the images of echelle spectrum order 77 of thorium - argon lamp are

provided. With such abundance of lines due to their small width defined generally by instrumental profile the number of lens hoods is not high that allows selecting the necessary number of single lines for exact wavelength calibration. As figure shows the width of a profile (FWHM) corresponds to about 2 pixels.

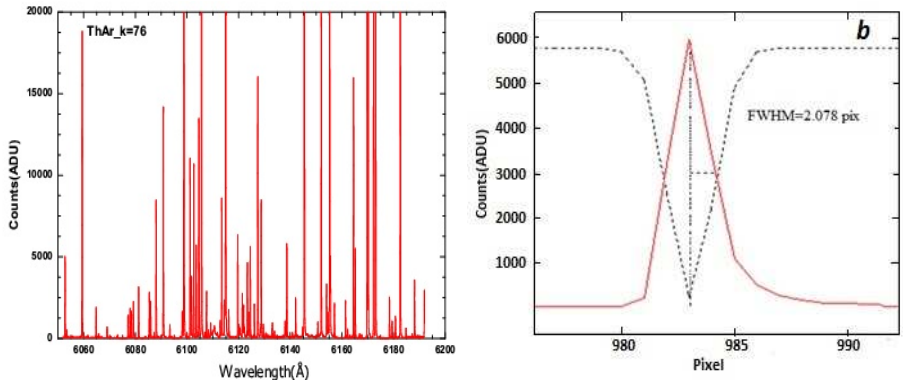

Fig. 8. Spectral region of ThAr lamp. a– spectrum of 77 order, b – instrumental profile.

9. OPERATION PROCEDURE WITH CCD IMAGES

1. We combine super-dark and subtract it from all the rest images (object, flat).

2. We combine super-flat from the serie of flats and super-comparison spectrum from the serie of comparison spectrum.

3. We extract the spectrum of object, flat and comparison spectrum simultaneously subtracting scattered light.

4. We look at the spectrum of object attentively. If there are defective pixels — we correct them. If cosmics are observed (usually at long exposures)- we remove them.

5. We normalize the flat: we exclude instrumental curve and spectral form of a plane field, only fringes and per-pixel heterogeneity remain.

6. We divide the spectrum of object to normalized flat.

7. We normalize the spectrum of object.

8. We plot a dispersive curve over the spectrum ThAr or Sky and create .fds (Full DiSpersion curve) files.

9. When loading the spectrum of object we specify .fds files, and the spectrum is opened in a wavelength scale. If the option AutoSelect FDS is on and FDS file is the only thing in this catalog – it will be chosen automatically.

10. We calculate instrumental displacement on the measured line-of-sight velocity of telluric lines and we enter this amendment into an option" Shift WaveScale for RV". The option "Auto RV-Shift" allows automatically considering (at loading stage) a shift in the scale of line-of-sight velocity which we entered last time for this spectrum.

11. The spectrum of object is ready for further analysis. If required, it is still possible to account heliocentric amendment.

10. BACKGROUND CORRECTION

Determination of scattered light level (or subtraction) is a part of the extraction procedure of a spectrum. In all spectrographs besides the spectrum of expanded radiation, some quantity of parasitic (scattered) radiation of other wavelengths always fall on output slit of the spectral camera. It can be explained with multiple light reflection from optical details, flares on their mounts and internal walls of the instrument, light scattering on surfaces of optical details. Scattered light reduces the accuracy of spectrophotometric measurements, in particular, when the brightness of sources is not high. To reduce the level of scattered light, we blacken mounts and internal walls using special coverings. Scattered light is subtracted by DECH program during extraction of a spectrum in data processing . It is enough for complete subtraction of a scattered light that creation of a level of background - "FitBackground" (crosscut) is correctly made for mask building (Fig. 9).

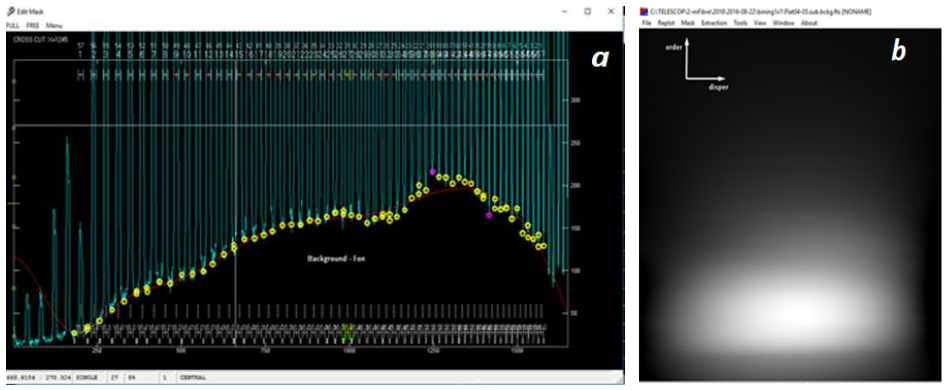

Fig. 9. Demonstration of scattered light. a – level of scattered light in X=1245. Yellow circles show the level of background between spectral orders. b- scattered light, subtracted from spectrum.

11. CORRECTION OF IMAGE DEFECTS

Spectrum orders conforming to red region with wavelengths more than λ 7000 Å may also contain so-called fringes representing a series of sharp low variations of intensity all over the order due to light interference in thin layers of transparent control electrodes of CCD matrix or in the crystal of silicon if it is thin. The example of a spectral order distorted by interference is given below (Fig. 10a).

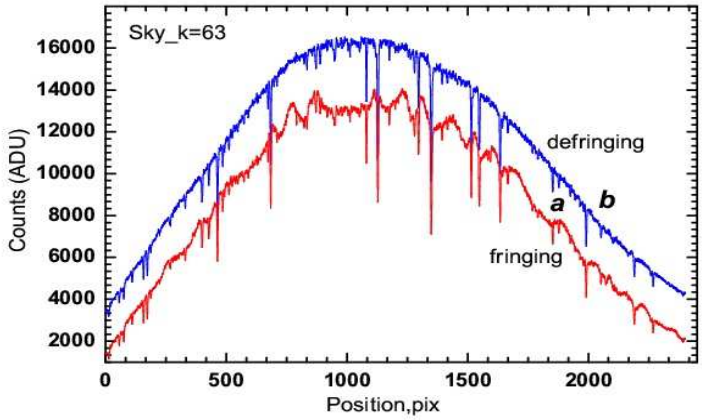

Fig. 10. Graphic image of echelle spectrum of order 63 distorted by fringes (a) and cleaned from fringes (b).

Effective way of releasing from these distortions is the method of dividing extracted spectrum into a calibration spectrum of a plane field (identical spectral orders). Fig. 10b shows spectral order 63 cleaned from fringe. In our spectrograph equipped with a thin CCD matrix ,amlitude of fringes doesn't excedd 1% in wavelength region shorter than λ6700 Å . Another feature of CCD unlike receivers of previous generations, was high sensitivity to so-called "cosmic" particles. The high-energy ions formed due to a collision of cosmic particles with molecules of the terrestrial atmosphere or disintegration of radioactive elements, facing with CCD matrix they knock out a large number of electrons. CCD matrix as a rule registers several hundreds of such events over the entire surface of a receiver in an hour. As it is provided in the program cosmic particles are removed by median addition of spectra in which pixel readings by noisy space particles, are improved.

12. CONTINUUM

Continuum is a responsible operation on which the further result of a spectral research depends. Correctness of a continuous spectrum level,especially in echelle spectrogms, to a large extent depends on researcher's proficiency. Even in the

era of photographic emulsions and common non-echelle low - dispersive spectra, normalization on the continuum of wide, first of all, hydrogen lines in spectra of A-F type stars was a problem. In particular, this task is a problem for echelle spectra. Width of spectral orders of echelle gratings operating in high orders is small. For example, the region of wavelength in echelle order 72 makes 96 Å (in $H\alpha$ lines). Therefore in spectra of hot stars with wide lines particularly in echelle orders where Balmer lines of hydrogen are located, the level of a continuous spectrum is sufficiently difficult and requires a special approach to this procedure. In the regions of strong blending (confluence of lines) or wide strong lines, the continuum may proceed even higher than the level of obtained spectrum. Continuum line, as a rule, is smooth and convex. If there are doubts in the correctness of the continuum in this order, energy distribution in adjacent orders of the spectrum can be compared. Intensity of adjacent orders in echelle spectra are close. As seen from Fig. 11a (k =72), spectral order level in the field of Hα line is lower than adjacent orders. Wide wings of Hα line don't permit to see the level of a continuous spectrum and if we perform a false continuum in this order, we will get wrong values of equivalent widths.

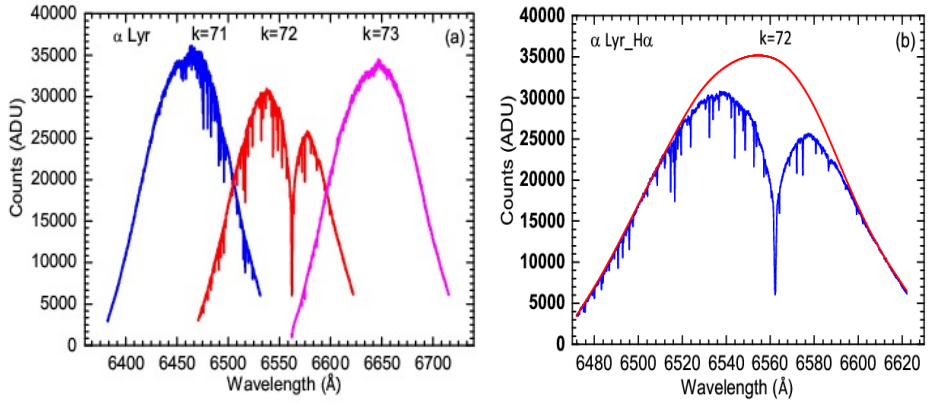

Fig. 11. 71-73 orders of echelle-spectrum of α Lyr, containing lines Hα (a); result of restoration of the continuum (b).

Large-size CCD was chosen intentionally to perform the continuum correctly in spectra of hot stars, particularly, in spectral orders where Balmer lines are located. For example, length of spectral region of order 72 (Hα region), free from adjacent orders, is found to be 96 Å . As Fig. 11 shows the length of a spectral order is actually 156 Å . This gives a chance to combine precisely the continuum curves of adjacent orders. As seen from Fig. 11 the maximum value of spectral orders comprising Balmer lines equals to average maximum value of adjacent orders. We indicate this value in the option "Mode-User Defined". Further, we

choose the continuum curves of adjacent orders. We shift this curve up to the maximum value. This curve can serve as a hint – where the continuum passes. As a result we will receive the restored continuum. Fig. 11b shows the result of restoration of the order containing Hα line in the spectrum of Vega - α Lyr.

13. TESTING THE POSITION AND PHOTOMETRIC CHARACTERISTICS OF THE SPECTROGRAPH

The spectrograph was tested in spectra with resolution of R = 56000.
1. Fiber-optic echelle spectrographs permits to measure radial velocities of celestial bodies with rather great accuracy. We have researched this spectrograph for accuracy of measuring radial velocities for spectral lines with various half widths (FWHM=0.14÷0.60 Å). For this purpose measurements were performed both on telluric lines, and on spectra of stars of different spectral classes. Telluric lines are narrow absorption lines in spectra of cosmic sources when their radiation passes through the terrestrial atmosphere. Width of these lines is close to width of an instrumental contour. Radial velocities of 108 telluric lines (FWHM=0.14-0.22Å) in the field of wavelengths $\lambda\lambda$5800-7400 ÅÅ on 9 echelle orders in a star spectrum of αCMi (Procyon) obtained in 26-11-2016 were measured. Results of the measurements are given in Fig. 12. Values of radial velocities show deviations of $\pm$ 60 m/s from average value. Standard deviation is σ = 36.28 m/s. As Fig. 12 shows the average value of radial velocities of telluric lines is almost preserved in the field of wavelengths $\lambda\lambda$5800-7400 ÅÅ.

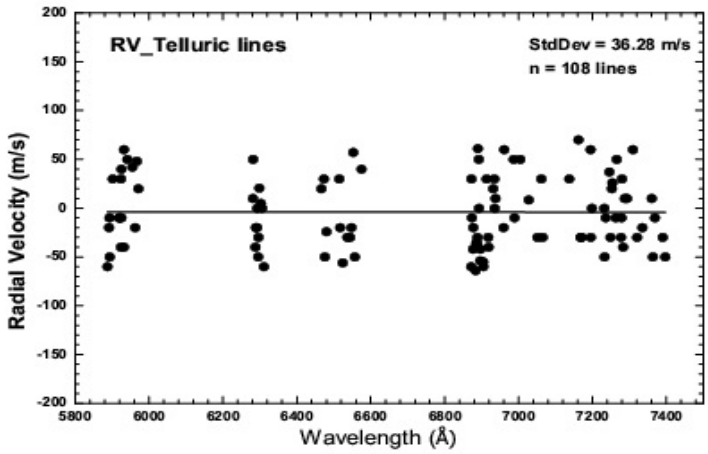

Fig. 12. Measured radial velocities of telluric lines in the spectrum of Procyon (α CMi).

Measurement results of radial velocities on atmospheric lines of stars.

α **CMi (Procyon).** Fig. 13a presents the measurement results of radial velocities for 309 lines (FWHM=0.20-0.25 Å) on 54 echelle orders in the field of wavelengths $\lambda\lambda 4000 - 7400$ÅÅ (S/N=300-400) in star spectrum of α CMi (Procyon) obtained in 29-11-2016. As the figure shows in this range of wavelength the value of radial velocities are constant, around average value of RV =-5429 m/s. Standard deviation is σ = 98.2 m/s. Data points of our measurements lie on a curve of radial velocities from [13] quite well (Fig. 13 b).

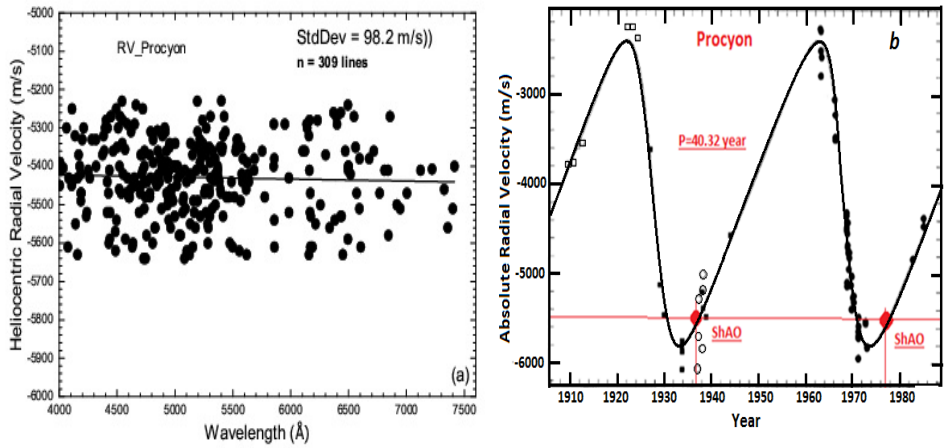

Fig. 13. Measured (on selected spectral lines) radial velocities of Procyon (a), Curve of radial velocities from Irwin et. al. [13], point of ShAO – our data (b).

43 Peg. Radial velocities were measured using 145 spectral lines (FWHM=0.20-0.40 Å) on 47 echelle orders, in the field of wavelengths $\lambda\lambda$ 3900-6400 ÅÅ in the spectrum (S/N=100-200) of a standard star 43 Peg obtained in 22-08-2016. Results of measurements are provided in Fig. 14a. Average value of radial velocities on our measurements: RV=8.56 km/s (in the database SIMBAD RV=8.5 km/s). Standard deviation is σ = 93 m/s.

α **Lyr.**Radial velocities were measured on 66 spectral lines (FWHM=0.5-0.6 Å) in the field of wavelengths $\lambda\lambda$3800-7800 ÅÅ in the star spectrum α Lyr (S/N=150-200) obtained in 15-05-2016 (Fig. 14b). Standard deviation is σ = 0.49 km/s. Average value of radial velocities on our measurements: RV =-13.47 km/s.

2. One of the important features of spectral devices of high resolution is the level of systematic and random errors of measurements of equivalent widths of lines. Equivalent widths of lines were measured on spectra with resolution of R=56000. The spectra was processed using advanced version of the software package DECH. The scattered light was subtracted in the extraction of echelle

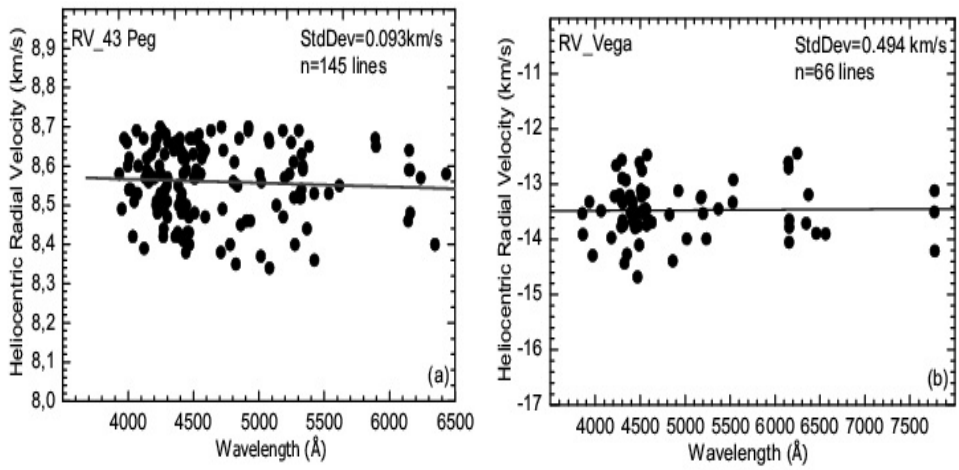

Fig. 14. Measured radial velocities (on selected absorption lines) of standard stars 43 Peg (a) and α Lyr (b).

orders. Spectra in red area ($\lambda > 6700$ Å) were cleaned from fringes (with division into flat). To measure equivalent widths mainly weak and average spectral lines were chosen (in the range of values of equivalent widths: 10-400 mÅ) from known literature sources. Equivalent widths were measured in three ways: direct integration; on Gaussian profile; with Voigt profile. Equivalent widths of strong and non-blended spectral lines were measured by direct integration. Equivalent widths of weak blended lines were measured on Gaussian profile. Voigt profile was used for the lines with depressive wings (NaD doublet, MgB triplet, etc.). In the spectrum of the star α Lyr equivalent widths of all lines were measured using the direct integration. Results of our measurements for equivalent widths on three standard stars (Procyon, Arcturus, Vega) were compared to similar data from literature.

Procyon. Fig. 15 shows the comparisons of equivalent widths measured by us on star spectra of Procyon (αCMi), for 110 spectral lines (in the range of values 10-400 mÅ) with data from [14–16]. Spectral resolution of literature data are similar to our data. In the spectra of Smith [14] and Edmonds [15] inverse dispersion is 4.8 Å/mm, but in the spectra of Allende Prieto 16 spectral resolution is R=60000. The difference in values of equivalent widths between our (ShAO) and the data from [14, 15] for some lines reaches up to 10%, but on 47 lines the standard deviation makes $\sigma = 7.15$ mÅ. Average values of measured equivalent widths between the data of ShAO and the data from the works [14, 15] match quite well: EW(ShAO) - EW (Smith, Edmonds) = - 1.35 mÅ. Spectra in works [14,15] were obtained in 1965 and 1981 and processed by classical methods. It is possible that, the difference in the values of equivalent widths is connected with

underestimation of scattered light in the spectrograph at a stage of processing classical spectra. The coincidence of values of equivalent widths between the data of ShAO and Allende Prieto can be practically considered indirect proof of this assumption [16]. Standard deviation is $\sigma = 2.39$ mÅ on 63 lines, the difference in values of equivalent widths makes only 3-5% and it is within limits of a measurement error. Spectra in [16] were obtained in 1999 with spectral resolutions of R=60000 and processed using IRAF program. Average values of equivalent widths practically coincides: EW(ShAO) - (EWAllende) =1.117 mÅ.

Constraint equations between our measurements and the data from [14–16] of equivalent widths of lines in the spectrum of Procyon (α CMi), is

$$\text{EW(ShAO)} = 0.991 \cdot \text{EW(Allende)} + 1.813;$$
$$\text{EW(ShAO)} = 0.99 \cdot \text{EW(Smith,Edmonds)} + 0.315$$

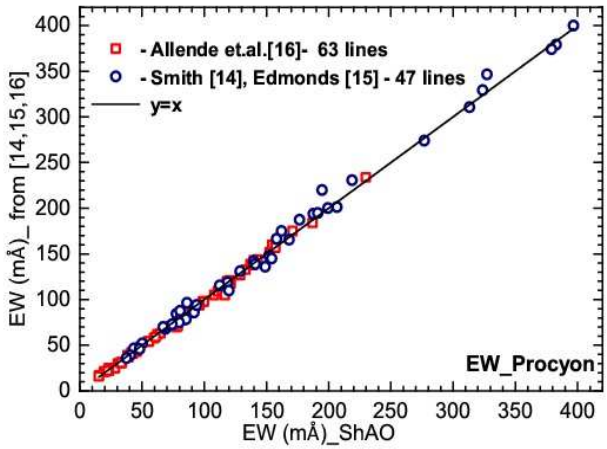

Fig. 15. Comparison of equivalent widths of Procyon. Direct line – graphic of function y=x.

Arcturus Equivalent widths (in the range of values $5 \div 300$ mÅ) were measured in the spectrum of standard star Arcturus (αBoo) for 114 lines and compared to similar literature data [17, 18]. Results of comparisons are given in Fig. 16. Measurement data of ShAO match well with the data of measurements of Ramirez, etc. [17], performed in 2011. The standard deviation for 38 lines makes $\sigma = 2.25$ mÅ. Average values of equivalent widths practically don't differ within a measurement error: EW(ShAO) - (EWRamirez) =0.961 mÅ. Comparison of the data of our measurements (ShAO) for 76 lines with the data of Mäckle, etc. [18], performed in 1975, shows systematic difference averagely to 8%. Values of the equivalent widths measured in ShAO are systematically overestimated compared with the measurements of [18]. The standard deviation for 76 lines makes:

σ = 5.81 mÅ. Difference of average values of equivalent widths: EW(ShAO) - (EWMackle) =4.7 mÅ.

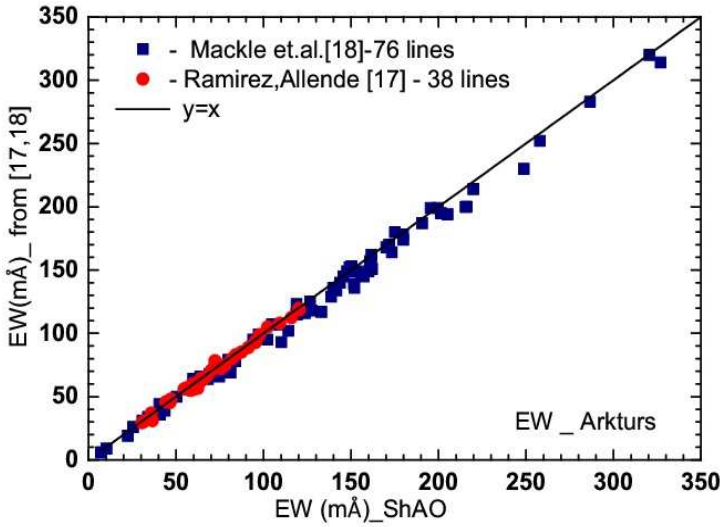

Fig. 16. Comparison of equivalent widths of Arcturus (α Boo). Direct line – graphic of function y=x. Spectra were processed using the programs DECH (ShAO) and IRAF [17] and classical method [18].

Constraint equations between our measurements and the data from [14–16] of equivalent widths of lines in the spectrum of Arcturus (α Boo), is

$$\text{EW(ShAO)} = 1.029 \cdot \text{EW(Mackle)} + 0.85;$$
$$\text{EW(ShAO)} = 1.008 \cdot \text{EW(Ramirez)} + 0.395.$$

Vega. Equivalent widths (in the range of values $10 \div 90$ mÅ.) for 36 lines were measured in a spectrum of Vega (α Lyr) and the results were compared to the data from [19]. Results of comparison are given in the Fig. 17. As the figure shows there is a certain variation in the values of equivalent widths between the measurements of ShAO and Qiu, etc. [19]. This variation can be partially related to the complexity of profile structures of spectral lines in spectrum of α Lyr. The standard deviation on 36 lines is: $\sigma = 2.38$ mÅ.

Deviations in the values of equivalent widths in some lines make about 10%, and their average values are rather similar:

$$\text{EW(ShAO) - (EWQiu)} = 1.6 \text{ mÅ}.$$

Constraint equations between our measurements and the data from [14–16] of equivalent widths of lines in the spectrum of Vega, is

$$\text{EW(ShAO)} = 1.008^*\text{EW (Qiu)} + 1.42$$

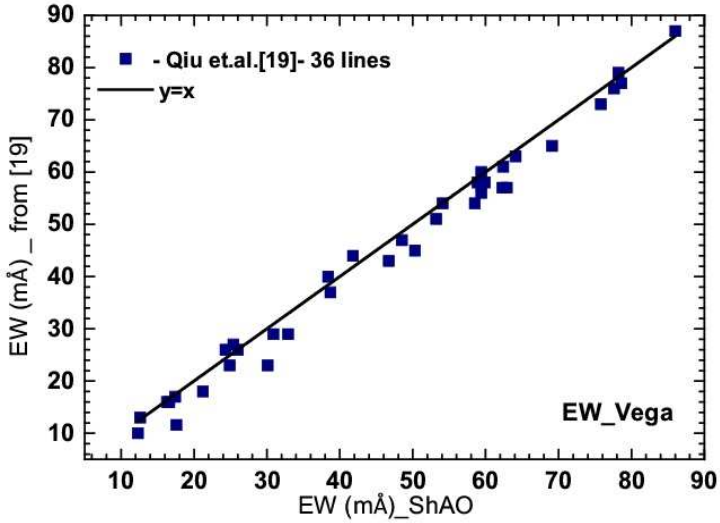

Fig. 17. Equivalent width of Vega. Direct line–graphic of function y=x. Spectra were processed using the programs DECH (ShAO) and MIDAS [19].

Spectral quality of spectra of ShaFES was estimated by comparing observed equivalent widths in the spectrum of standard stars with literature data [14–19]. As seen from the constraint equations inclination is close to the unit and small values of a zero point (0.315 - 1.813) indicate that the equivalent widths measured by us systematically are more than the similar literature data.

14. CONCLUSIONS

The 2-m telescope of ShAO of NAS of Azerbaijan was built and applied in the observation of fiber-optic echelle spectrograph with high resolution within the framework of the program for modernization and improvement of the park of the scientific equipment. The spectrograph operates in two modes ($\Delta\lambda/\lambda$=56000 and 28000). Transition from one mode to another occurs for several seconds. Instrumental displacement does not occur due to immobility and compact design of the spectrograph and also the light given from the object and the same channel and from calibration lamps. Spectra of thorium - argon (Th-Ar) lamps and Sky were used as a comparison spectrum. Width of narrow non-blended lines of Th-Ar lamps is practically defined by the width of an instrumental contour. Width of an instrumental profile (FWHM) conforming to 2 pixels was estimated for these lines. Measurement accuracy of radial velocities is very high (several 10 m/s). Measurement error of equivalent widths is 1-5%. Guiding of observed objects is semi-automatic and their images are transferred to the observational room.

Large CCD camera with nitrogen cooling, 4000×4000 pixels is used as a light detector that allows obtaining a large optical range ($\lambda\lambda$3700-8500 ÅÅ) in one frame ($\lambda\lambda$ 3600 $\div$ 9000 ÅÅ). Optimum operating range of wavelengths is $\lambda\lambda$3700-8500 ÅÅ. Cross-disperser does not permit a wavelength less than λ 3700 Å, but strong fringes appear in the field of wavelengths of more than λ8500 Å. This paper describes an effective method of cleaning spectra from fringe by dividing extracted spectra into a calibration spectra (in identical spectral orders). It is known that correct performance of continuous spectra is a problem for echelle spectra, in particular, in those spectral orders where they contain lines with wide wings (for example, Balmer lines of hydrogen). This question was reviewed in this work. On the example of a spectrum of α Lyr we have tested the restoration technique of true level of the continuum in 72 spectral order comprising Hα line. To facilitate this procedure the length of this order was purposely selected to 156Å.

Results of the comparative analysis of positional and photometric characteristics of this spectrograph with similar literature data showed that this complex is quite suitable to perform high-precision researches of the atmospheres of brighter stars (to $8^m - 10^m$ stellar magnitudes depending on spectral resolution mode); spectral monitoring of stars with different spectral features (young stars with small and intermediate masses, symbiotic stars, spectrally double and multiple stars, etc.); researches of supergiant stars to detect temporary features of stochastic stellar wind; astroseismological researches; researches of stellar magnetism; spectral researches of bodies of solar system, etc.

ACKNOWLEDGMENTS

Authors express deepest thanks to the reviewer for attentive reading our manuscript and valuable comments for improvement of manuscript, both on "scientific character", and manuscript format.

REFERENCES

1. Musaev, F.A., Coude echelle spectrometer. 1993, Astron. Lett., 19, 315

2. Rzayev, A.Kh., Mikailov, Kh.M., Alakbarov I.A., et al. 1999, Circular of ShAO, 95, 3

3. Mikailov, Kh.M., Khalilov, V.M., Alakbarov, I.A. Echelle-spectrometer of the focus Cassegrain of the 2-m telescope of ShAO. 2005, Circular of ShAO, 109, 21

4. Furenlid, I. & Cardona, O.A CCD spectrograph with optical fiber feed. 1988, PASP, 100, 1001

5. Pfeier, M.J., Frank, C., Baumuller, D., et al. FOCES-a fibre optics Cassegrain echelle-spectrograph. 1998, A&AS, 130, 381

6. Panchuk, V.E., Yushkin, M.V., Yakopov, M.V. High-Resolution Fiber-Fed Spectrographs. 2011, Astrophys. Bull., 66(3), 355

7. Valyavin, G.G., Bychkov, V.D., Yushkin M.V., et al. High-Resolution Fiber-Fed Echelle Spectrograph for the 6-m Telescope. I. Optical Scheme, Arrangement, and Control System. 2014, Astrophys. Bull., 69(2), 224

8. Panchuk, V.E., Yushkin M.V., Klochkova V.G., et al. Design of a High Resolution Spectrograph for the SAO 1-m Telescope. 2015, Astrophys. Bull., 70(2), 226

9. Bonev, T. Markov, H. Tomov, T., et al. ESpeRo: Echelle Spectrograph Rozhen. 2017, Bulgarian AJ, 26, 67

10. Peysakhson, I.V. Optics of spectral devices. 1975, 2, Leningrad, Mechanical engineering, 196

11. http://www.astro-cam.com/

12. http://www.gazinur.com/DECH-software.html

13. Irwin, Alan W., Fletcher, J.M., Yang, Stephenson L.S., et.al. The orbit and mass of Procyon. PASP, 1992, 104(677), 489

14. Smith, G. Non-resonance lines of neutral calcium in the spectra of the sun and Procyon. 1981, A&A, 103(2), 351

15. Edmonds, Feank N., Jr. A Spectrophometric Analysis of Procyon. I. Equivalent Widths and Line Profiles. 1965, ApJ, 142, 278

16. Allende, Prieto, Carlos; Asplund, Martin; García López, Ramón J.; Lambert, David L. Signatures of Convection in the Spectrum of Procyon: Fundamental Parameters and Iron Abundance. 2002, ApJ, 567(1), 544

17. Ramírez, I., Allende Prieto, C. Fundamental Parameters and Chemical Composition of Arcturus. 2011, ApJ, 743(2), 135, 14

18. Mäckle, R., Griffin, R., Griffin, R., Holweger, H. A model-atmosphere analysis of the spectrum of Arcturus. 1975, A&AS, 19, 303

19. Qiu, H.M., Zhao, G., Chen, Y.Q., Li, Z.W. The Abundance Patterns of Sirius and Vega. 2001, ApJ, 548, 953

ŞAMAXI FİBRE EŞELLE SPEKTROQRAFI: ShaFES

X. M. Mikayılov [a]***, F. A. Musayev*** [b]***, İ. Ə. Ələkbərob*** [a]
B. N. Rüstəmov [a]***, O. V. Xəlilov*** [a]

[a] *N.Tusi adına Şamaxı Astrofizika Rəsədxanası, Azərbaycan Milli Elmlər Akademiyası, Şamaxı rayonu, Azərbaycan*

[b] *Xüsusi Astrofizika Rəsədxanası, Rusiya Elmlər Akademiyası, Nijniy Arxız, Rusiya*

Məqalədə Şamaxı Astrofizika Rəsədxanasının 2-m teleskopunun Kasseqren fokusu üçün hazırlanmış yüksək ayırdetməli optik lifli eşelle spektroqrafın təsviri verilmişdir. Spektroqrafın prinsipial optik sxemi və onun teleskopa asılan hissəsinin sxematik təsviri təqdim olunur. Spektroqraf $\lambda\lambda$ 3700-8500 ÅÅ dalğa uzunluğu oblastında, spektral ayırdetməsi 28000 və 56000 olan iki rejimdə işləyir. Spektroqrafın fotometrik (spektral xətlərin ekvivalent eni) və mövqe (xətlərin şüa sürətlərinin təyini) xarakteristikalarının sınaq testlərinin nəticələri analiz olunur.

Açar sözlər: Cihaz və qurğular – Spektroqraf

LOW STATE OF RADIATION IN EMISSION SPECTRUM OF THE STAR MWC 361

N. Z. Ismayilov*[*], *O. V. Khalilov*, *S. A. Alishov

Shamakhy Astrophysical Observatory named after N.Tusi,
Azerbaijan National Academy of Sciences, Shamakhy region, Azerbaijan

Results of spectral researches of spectral-binary Be Herbig type star MWC361 are presented. Observational phases are corresponding to the minimum of the radial velocity curve of the system. Emission hydrogen lines Hα and Hβ show the low condition of radiation. First time in the spectrum we have discovered diffuse interstellar bands DIB $\lambda\lambda$ 5780, 5797 Å. For 3 months of observations we have discovered a considerable increase of relative intensities of emission lines components of hydrogen and in emission lines Si $\lambda\lambda$ 6347 6371 Å and [OI] $\lambda\lambda$ 6300, 6363 Å.

Keywords: Ae/Be Herbig type stars, – Emission spectrum – Circumstellar matter – Variability – MWC 361

1. INTRODUCTION

In the whole, Ae/Be Herbig (HAEBES) stars and classical T Tauri (CTTS) type stars have such common observational properties as infrared radiation (IR) excesses indicating the existence of the circumstellar gas-dust disk [8, 19], or excesses in the ultraviolet (UV) and optical ranges, which are considered indicators of accretion of mass on the star [6,11,12]. Resolved strong and forbidden emission lines in the spectrum are also observed in both groups of stars [1, 21]. Despite the similarity of many properties in HAEBES and CTTS stars, it is still unclear whether the ways of interaction of the circumstellar matter in these star groups with the central star are identical. There are works in which arguments are given in favor of the difference in the mechanisms of interaction of the circumstellar matter with the central star [15, 17]. To elucidate these questions, further detailed studies of the physical characteristics of individual HAEBES stars are needed.

[*] E-mail: ismailovn@yahoo.com

The purpose of this work is to study the time variations of various spectral indicators of circumstellar matter in the spectrum of the star MWC 361.

2. THE OBSERVATIONAL MATERIAL AND RESULTS

Spectral observations were performed in the focus of Cassegrain of the 2 m telescope of ShAO of the Azerbaijan National Academy of Sciences. An echelle spectrometer operating on the basis of the UAGS spectrograph [14,24] was used. As a light detector, a CCD with 530×580 elements was used. Observations of program stars were carried out in the range $\lambda\lambda 4700 - 6700$ Å. The spectral resolution is R = 14000. The signal to noise level in the region of the line Hα was S/N=80–100 averagely, and in the region of the $H\beta$ line, S/N = 10-20. For May-September 2016, 15 pairs of echelle spectrograms of the star were obtained. The method of observations and material processing is described in more detail in the work of Ismailov et al. [14].

The errors in the intensity measurement due to the continuum, depending on the S/N level, were 0.5-1% in the region of the line Hα and up to 2-4% in the region of the line Hβ. The limiting value of the equivalent width, which can be measured confidently in the red part of the spectrum, is 0.03 Å. The average error in measuring the radial velocities for individual lines in the spectra of standard stars does not exceed ± 1.5-2.5 km/s.

According to Altamore et al. [3] and Bašek et al. [5], the bright component of the MWC 361 (HD200775) system has a spectral class B3Ve. This is one of the brightest Be Herbig type stars and is known as a spectral binary with an orbital period around $P \approx 1345$ days [20]. The data of six different authors on the solutions of radial-velocity curves of the system differ significantly each from other [2, 7, 9, 13, 18, 20] which makes it necessary to rebuild the radial velocity curve of individual components of the system.

Our observations were made in June-September 2015 and correspond to the phases 0 ± 0.3 in the radial-velocity curves given by different authors. In Table 1, the top line contains references to the authors' work, the second line shows the phases calculated by us for the elements obtained by these authors, and in the third line the average values of these phases are given. In such phases, the spectra of the star are of interest for studying individual spectral lines that form in the near and far parts of the circumstellar disk from the central star.

Fig. 1 shows the fragments of different ranges of the stellar spectrum. The left low panel contains the range of Si II λ 6347, 6371 Å and [OI] 6363 Å emission lines. The spectral range containing forbidden line [OI] λ 6300 Å is placed in the top right panel. We have detected diffusion interstellar bands (DIBs) λ 5780 and 5797 Å (the left top panel) in stellar spectrum. Our spectral resolution does not

Table 1. Phases of our observations calculated on orbital elements provided by different authors

Author	Pogodin et al. (2004)	Ismailov (2003)	Bisyarina et al. (2015)	Beristy et al. (2013)	Monnier et al. (2006)	Alecian et al. (2008)
Interval	0.988 – 0.057	0.255 – 0.335	0.832 – 0.900	0.734 – 0.799	0.829 – 0.897	0.798 – 0.865
Average	0.026	0.299	0.870	0.769	0.866	0.835

allow separating the structure of some components of these lines. It is interesting that Pogodin et al [20] in their work have been presented profiles of ion Si II λ 4128, 4131 Å which unlike Si II λ 6347, 6371 Å lines according to our observations have a pure absorption profile.

[OI] $\lambda\lambda$ 6300 and 6363 Å lines are confidently separated from noise. Equivalent widths of [OI] λ 6363 Å line show significant scatter from an average 0.098 $\pm$ 0.056 Å. Average value of equivalent widths of the line is in good agreement with the data of Hernandez et al. [23]. The radial velocities of the line were determined by the displacement of the emission peak at the half of intensity level. [OI] λ 6300 Å line shows diffusion emission with an equivalent width of 0.087 $\pm$ 0.033 Å, and any structure in this line as well as in [OI] λ 6363 Å line can't be detected. As seen from the right top panel of fig.1 that near [OI] λ6300 Å line there are rather intensive telluric lines, the positions of which (O2 $\lambda\lambda$6292.1621, 6295.179, 6305.8101 Å and H2O $\lambda\lambda$ 6292.6136, 6294.6473, 6302.005 Å) are shown with vertical segments.

On our spectrograms Hα and Hβ line profiles have a double peak emission, divided by the central absorption. The general structure of line profiles did not show significant variations during our observations. However, the intensity ratio of a blue component to red V/R shows by wavy-like variation. In fig. 2 the diagram of V/R parameter versus of time for Hα and Hβ lines is presented. As it is seen at the beginning of observations intensity ratio of the blue component to red in Hα is about 1, and by the end of the season this ratio became equal to about 1.3, but in Hβ line it is about 2. Such variation occurs for about 90 days.

Thus, in spite of the fact that the period of the system is quite large (3.68 years), for 3 months a significant variation in the intensities of emission peaks in Hα and Hβ lines is observed. Rather, such variations are not related to the orbital motion of the components.

To reveal the variable part of the profile in the line Hα, at first we averaged the line profiles and obtained a seasonally average profile, in the wavelength reduced to the sun. At the same time, the displacement of the line for the orbital motion was not taken into account; for the observed period of time, the line displacements

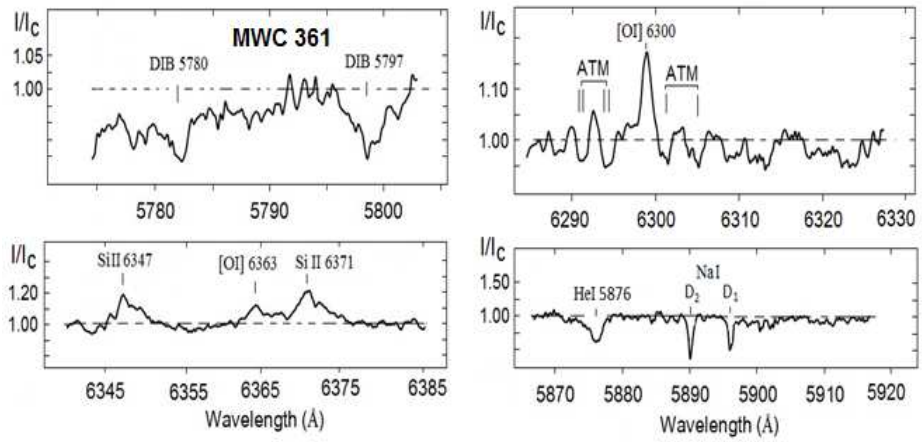

Fig. 1. Some fragments of MWC 361 spectrum.

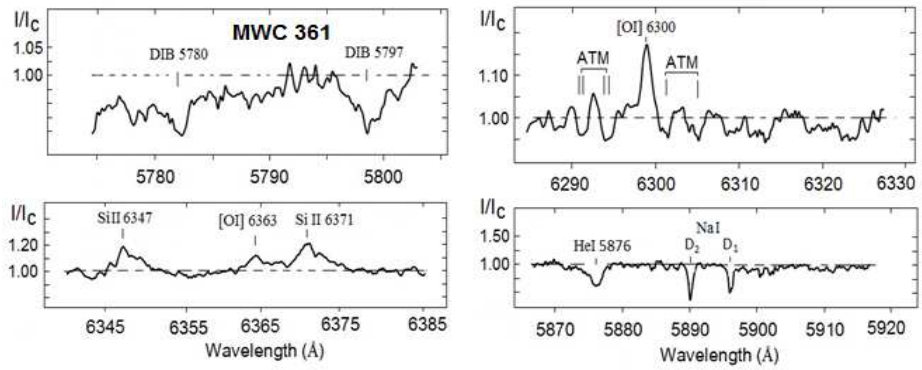

Fig. 2. A time variability of relation V/R for the blue and red components of Hα and Hβ emission lines.

should be negligible. In the left panel of Fig. 3, the average profile of the line Hα is shown as the average of the all observation time. Then all line profiles of different dates are divided into the average profile. The left panel of Fig. 3 shows the residual structure of the Hα line profile obtained for each night. Here I is the intensity of the profiles for each night, Im is the intensity of the average profile at the given wavelength. From this it can be seen that the structure of the residual profile varies considerably for different dates.Interestingly, both at the beginning and at the end of the season, the most intensive peaks in the residual profile have displacements from 0 to -45 km/s. After this, we calculated the standard deviation Σ from the mean of residual profiles. The left low panel in Fig. 3 shows the variation of Σ versus the wavelength. In the same place, the dotted line shows a

threefold noise level 3σ of Σ. As can be seen, the largest variation occurs in the central part of the profile, within the interval of about 10 Å.

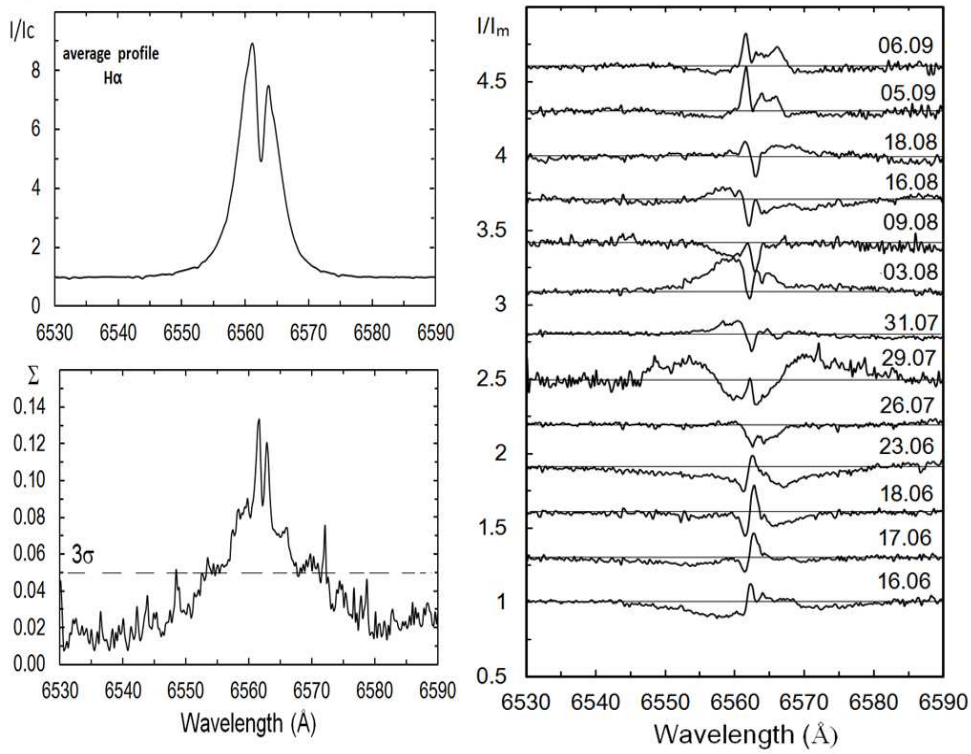

Fig. 3. In the top left: averaged Hα profile line for different nights of observations. Right panel: residual profiles for separate nights of observations, obtained by division of each profile to average. In the below left: standard deviation of Σ of relative intensity I/Im versus of wavelength for all residual profiles. Here I – profile intensity for each night, Im – average profile intensity at given wavelength. 3σ level shows triple value of mean-square error of measurements of a relative intensity.

Fig. 4 shows the diagrams of time variation in radial velocities and equivalent widths of the individual components of the line Hα. The designations correspond to: Vr1, Vr2 displacements of individual emission peaks, Vra is the displacement of absorption between the peaks, and Vr1/2 is the line shift at half the intensity. Mean values of these parameters, according to our observations, were -68, 50, -2 and -25 km/s, respectively. As it can be seen from Fig. 4, the radial velocities of the individual components of the line showed fluctuations reaching up to 20 km/s. The mean value of the radial velocity at the half intensity (bisector velocity) corresponds to - 20 km/s. According to the data of Pogodin et al. [20], this velocity was obtained in phase 0.0 along the radial velocity curve, constructed on

the line Hα and on the photospheric lines. According to the same Beresty et al. (2013), this displacement should occur near the 0.90P phase.

The average value of the total equivalent width of the line Hα, according to our observations, is about W $\lambda \sim 57$ Å for the standard deviation from the mean to ± 3.41 Å, which is about 5.9% of the average value of W. As evidenced by the data of other authors the value W $\lambda \sim 57$ Å is minimal, as shown in Pogodin et al. (2004), the equivalent widths of the line Hα during the orbital period show a variation in the range of 50-120 Å and reach a minimum at JD 24551500 (at the phase 0.75 according to Pogodin et al. [20]). Our observations showed that, as in the case of relative intensities (Fig. 2), a slight increase in the equivalent widths is observed after the date of JD 2457230.

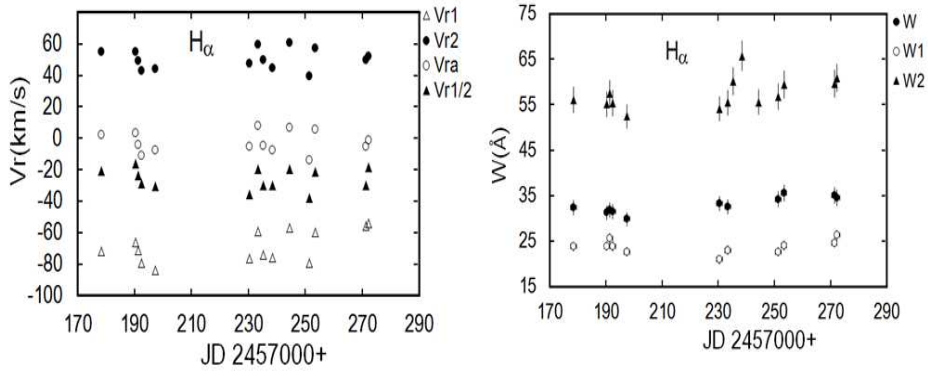

Fig. 4. Variation of radial velocities (left panel) and equivalent widths (right panel) of some components of emission Hα line. Symbols correspond to: Vr1 , Vr2 displacements of separate emission peaks, Vra – the shift of the central absorption and Vr1/2 – line shift at half-intensity level, W1, W2 and W – equivalent widths of blue and red components and full equivalent width of emission in Hα.

In Fig. 5 for example, the time dependence of the radial velocities (left panel) and equivalent widths (right panel) of the emission line Si II λ6371 Å is given. As can be seen from Fig. 5, the parameters of the line are varied from night to night. After JD 2457230, the equivalent widths are increased and the lines are displaced to the red part of the spectrum.

Fig. 6 shows a similar plot for the parameters of the [OI] λ6363, 6300 Å lines. As can be seen from this figure, the radial velocities in the low state of the radiation have an average value of about -10 km/s, but after the date JD 2457230 the Vr displaced mainly in the blue part of the spectrum. This is clearly visible from the values of the radial velocities of the [OI] λ 6300 Å line.

The line profile of HeI λ5876 Å is purely absorbing and does not differ from previous profiles obtained in our observations [13]. As noted by Ismailov [13],

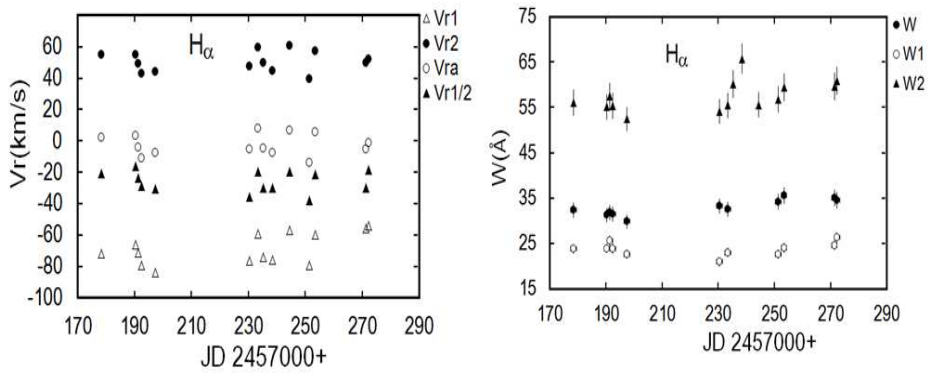

Fig. 5. Temporary dependence of radial velocities (left panel) and equivalent widths (right panel) of Si II $\lambda\lambda$6347 and 6371 Å emission lines. Open circles on the left panel correspond to the velocities of intensive peak, dark circles correspond to the velocities of the central line at a half-intensity level.

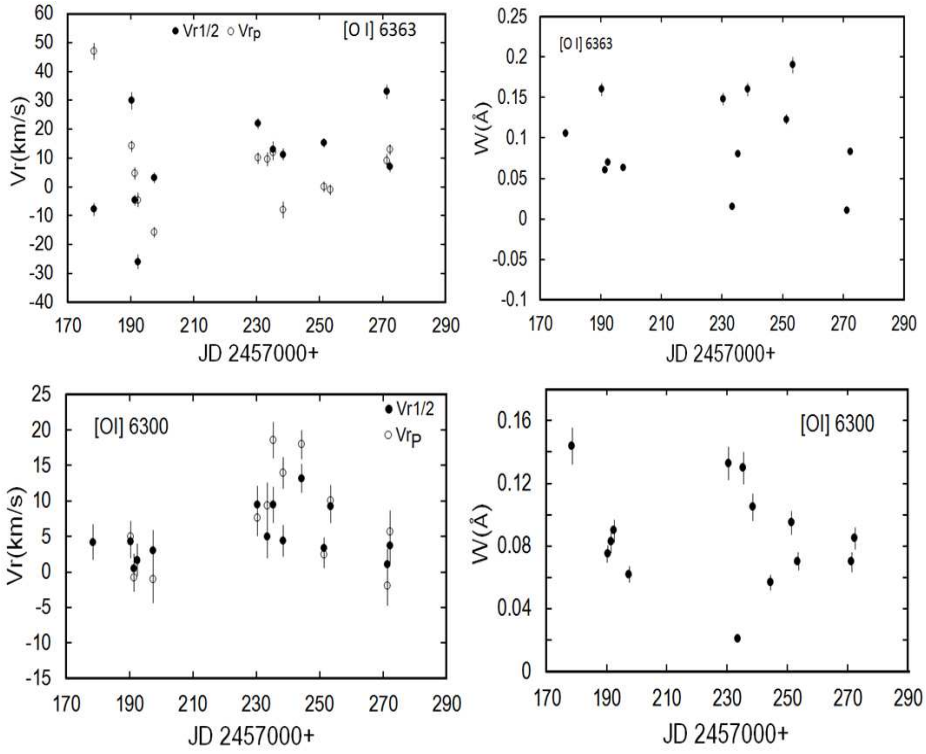

Fig. 6. The same as in Fig. 5 for the [OI] $\lambda\lambda$ 6300 and 6363 Å lines.

the line profile shows a variation in the steepness and width of the red or blue wing. In the spectrograms presented here, the blue wings of the line are widened.

Apparently, such variation is due to the orbital motion of the components in the binary system. Perhaps the secondary component of the system also gives a certain contribution of radiation to the helium line. This assumption is consistent with the opinion of Bisyarina et al. [9], who assumed that the second component of the system is also a B-star.

Fig. 7 shows a diagram of the variation of radial velocities and equivalent widths in the line He I λ5876 Å. The average value of radial velocities for this line at an equivalent width of 0.7 Å was obtained at 7 km/s. As it can be seen, there is a small scatter of values in both Vr and W_λ.

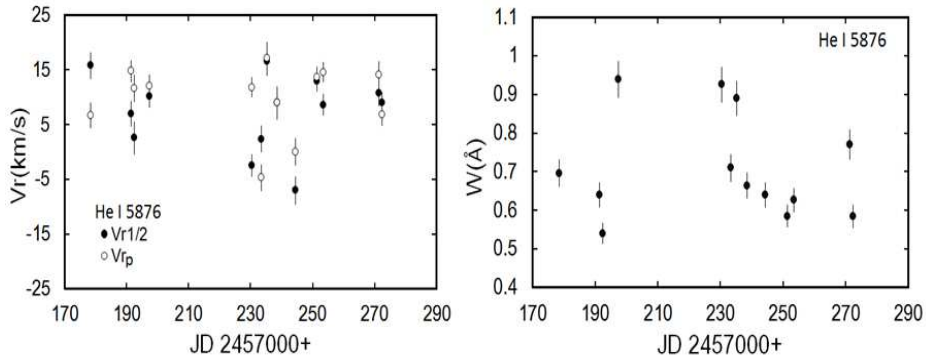

Fig. 7. The same as in Fig. 5 for the HeI λ 5876 Å line.

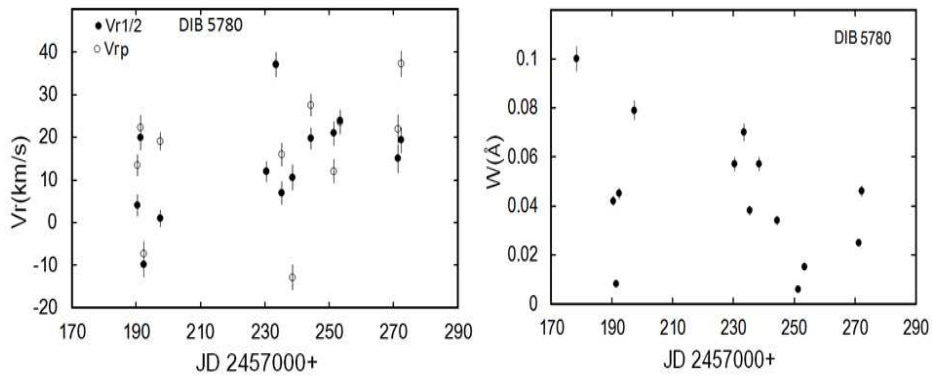

Fig. 8. The same as in Fig. 4 for DIBs λ 5780, 5797 Å.

In the spectrum of the star, narrow D1, D2 NaI lines are observed (Fig. 1, right low panel) with an average displacement of -12 ± 2.0 km/s to the blue part of the spectrum. The average value of the equivalent widths of the D1, D2 Na I lines was 0.27 ± 0.04 Å and 0.29 ± 0.03 Å, respectively. The ratio of the intensi-

ties of these lines is close to one, which indicates the optically thick or combined nature of the emitting regions in these lines. Significant variations during our observations in the D NaI lines are not detected.

In the spectrum of the star, we have firstly observed lines of interstellar origin DIB λ 5780, 5797 Å (Fig. 1). The first of these bands on individual dates of observation is much weakened and hardly stands out from the noise. The second band is more confident. We used the wavelengths of these bands λ5780.37 Å and λ5796.96 Å, which are given in the work of Klochkova and Chentsov [16]. The average value of the parameters and the standard deviation from the mean of these lines are: radial velocities 13 $\pm$ 18, 5 $\pm$ 22 km/s, and equivalent widths of 0.044 $\pm$ 0.03 Å and 0.035 $\pm$ 0.015 Å, respectively. According to the data of different authors [10,22], the ratio of the equivalent widths of these bands in different directions of the Galaxy is 2-3. In the spectrum of the star, the ratio of the values of equivalent widths of interstellar bands DIB λ 5780, 5797 Å is obtained within 1.2-3. The reason of such variations in the DIB lines is not entirely clear. Perhaps we see a variation in physical conditions in the circumstellar medium under the influence of the activity of the central star.

The time variation of the radial velocities and equivalent widths of the bands DIB λ 5780, 5797 Å have been shown in the Fig. 8. As it can be seen, on the whole, the observed character of the variation is the same as for the Si II and [OI] lines, which indicates their definite interrelation.

3. CONCLUSIONS

Thus, our spectral observations of Ae/Be Herbig type spectral-binary system MWC361 are interesting because they were obtained at the minimum moment of the radial velocity curve.

According to the data of different authors, the longitude of the periastron of the system has a value of $\omega = 200 - 250^{\circ}$ (see, for example, Bisyarina et al. [9] and references therein). With this orbit orientation, the minimum of the radial velocity curve corresponds to the moment of passage of the star near the periastron. The second component of the system is far away enough from the primary component.

Observations show that some T Tauri binary stars (for example, in DQ Tau Basri et al. [4]) demonstrated an increase in emission activity near the periastron, which may be a sign of asymmetric accretion. Beresty et al. [7] suggested that the reason of the increase in Hα emission in periastron can be the result of accretion onto the disk of the primary component. Perhaps the main reason for the gradual variation in the equivalent widths of the emission lines Hα and Hβ is the perturbation that occurs when the system components approach to the periastron. In

our case, the values of the equivalent widths of the hydrogen emission lines are minimal, which confirm our assumption.

According to Pogodin et al. [20], the values of the equivalent widths of the line Hα have $W_\lambda(H\alpha) \geq 80$ Å only in the time range of 2451800-JD2452250, i.e. for 450 days, which is about a fourth of the orbital period. For the rest of time, the Hα line shows a lower radiation state. In this case, the course of variation in equivalent widths occurred smoothly. According to the data of Pogodin et al. [20], the boundaries of the indicated time interval of the active state of radiation correspond to the phase interval 0.977P-0.312P, respectively. On the data of Table 1, the phases of our observations enter to this interval, but the values of the equivalent widths correspond to the low state. Apparently, it is necessary to clarify the value of the period and elements of the system's orbit. Note that according to Bisyarina et al. [9], the last period of the minimum of equivalent widths values of the line Hα corresponds to the interval JD2456600-JD2456800, which corresponds to the phases of the period 0.556P-0.705P for the elements of Pogodin et al. (2004). In other words, in 2013-2014, the intensity of emission in the line Hα was observed in minimum. Our 2015 data show the continuation of the minimum radiation in this line. We assume that in 2016 the equivalent width in the emission line Hα is expected to increase, at least to the level of 2012 ($\sim$ 92 Å, according to Bisyarin et al. [9]).

Observations showed that after JD 2457230 main variations occurred in the circumstellar structure of the star. The relative intensities of the emission components in Hα and Hβ lines increased, the displacement of some SiII $4\lambda\lambda 6347, 6371$ Å emission lines and the DIB $\lambda\lambda$5780, 5797 Å absorption bands are displaced to the red part of the spectrum, and their equivalent widths also increased at this time. Starting from this date, the radial velocities of the [OI] $\lambda\lambda$ 6300, 6363 Å lines have shown a tendency to shift to the blue part of the spectrum. Our results showed that there is a rapid variability in both emission and absorption spectra of the star during a period of about 90 days. This is only 0.067 part of the orbital period. The reason for such variations may be different processes that are not related to the orbital motion of components, for example, such activity as matter ejections, pulsations in the star itself, and accretion in the circumstellar disk of components. A slight variation in both the forbidden oxygen lines, in the bands of interstellar origin DIB $\lambda\lambda$5780, 5797 Å, indicates time variability in the physical conditions in outermost parts of the circumstellar structure.

The HeI λ5876 Å is an absorption line and features of the emission components in our spectra are not separated. If the system really consists of two B-stars, then near the periastron the total value of the equivalent widths of helium photospheric lines belonging to individual B-stars of the system would be relatively constant. In this case, the reason for variation the equivalent widths of the helium line are

not entirely clear. The asymmetric expansion of the blue or red wing of the line observed by us at certain times [13] is also not completely clear.

ACKNOWLEDGMENTS

The work is supported by the project on priority research areas of the Azerbaijan National Academy of Sciences.

REFERENCES

1. Alencar, S.H.P. & Basri, G. Profiles of Strong Permitted Lines in Classical T Tauri Stars. 2000, AJ, 119, 4, 1881

2. Alecian, E., Catala, C., Wade, G.A., et al. Characterization of the magnetic field of the Herbig Be star HD200775. 2008, MNRAS, 385, 1, 391

3. Altamore, A., Baratta, G.B., Casatella, A., et al. Ultraviolet, optical, and infrared observations of the Herbig Be star HD 200775. 1980, A&A, 90, 3, 290

4. Basri, G., Johns-Krull, C.M., Mathieu, R.D. The Classical T Tauri Spectroscopic Binary DQ Tau. II. Emission Line Variations with Orbital Phase. 1997, AJ, 114, 781

5. Baschek, B., Beltrametti, M., Koppen, J., Traving, G. On the Spectrum of the Herbig Be-Star HD200775. 1982, A&A, 105, 300

6. Boehm, T. & Catala, C. Rotation, winds and active phenomena in Herbig Ae/Be stars. 1995, A&A, 301, 155

7. Benisty, M., Perraut, K., Mourard, D. et al. Enhanced Hα activity at periastron in the young and massive spectroscopic binary HD 200775. 2013, A&A, 555, 113, 10

8. Bertout, C., Basri, G., Bouvier, J. Accretion disks around T Tauri stars. 1988, ApJ, Part 1, 330, 350

9. Bisyarina, A.P, Sobolev, A.M., Gorda, S.Yu., Parfenov S.Yu. Optical spectroscopic monitoring of the Herbig Be binary star HD 200775: New maximum of activity and refinement of the orbital period. 2015, Astrophys.Bull., 70, 3, 299

10. Galazutdinov, G.A., LoCurto, G., Krelyowski, J. High-Resolution Profiles of Diffuse Interstellar Bands. 2008, ApJ, 682, 2, 1076

11. Dodin, A.V., Lamzin, S.A. Interpretation of the veiling of the photospheric spectrum for T Tauri stars in terms of an accretion model. 2012, Astron. Lett., 38, 10, 649

12. Donehew, B., Brittain, S. Measuring the Stellar Accretion Rates of Herbig Ae/Be Stars. 2011, AJ, 141, 46

13. Ismailov, N.Z. The Herbig Ae/Be Star HD 200775 as a Spectroscopic Binary. 2003, Astron. Rep., 47, 3, 202

14. Ismailov, N.Z.,.Bahaddinova, G.R, Khalilov, O.V., Mikailov, Kh.M. Spectral variability of IL cephei. 2013, Astrophys.Bull., 68, 2, 196

15. Cauley, P.W. & Johns-Krull, Ch.M. Diagnosing Mass Flows around Herbig Ae/Be Stars Using the He I λ 10830 Line. 2014, ApJ, 797, 112

16. Klochkova, V.G. & Chentsov, E.L, The Optical Spectrum of an LBV Candidate in the Cyg OB2 Association. 2004, Astron. Rep., 48, 12, 1005

17. Malfait, K., Bogaert, E., Waelkens, C. An ultraviolet, optical and infrared study of Herbig Ae/Be stars. 1998, A&A, 331, 211

18. Monnier, J.D., Berger, J.-P., Millan-Gabet, R., et al. Few Skewed Disks Found in First Closure-Phase Survey of Herbig Ae/Be Stars. 2006, ApJ, 647, 444

19. Natta, A., Prusti, T., Neri, R., et al. A reconsideration of disk properties in Herbig Ae stars. 2001, A&A, 371, 186

20. Pogodin, M.A., Miroshnichenko, A.S., Tarasov, A.E., et al. A new phase of activity of the Herbig Be star HD 200775 in 2001:Evidence for binarity. 2004, A&A, 417, 715

21. Finkenzeller, U., Rotational velocities, spectral types, and forbidden lines of Herbig Ae/Be stars. 1985, A&A, 151, 340

22. Herbig, G.H. The Diffuse Interstellar Bands. 1995, ARA&A, 33, 19

23. Hernandez, J., Calvet, N., Bricen, C., et al. Spectral Analysis and Classification of Herbig Ae/Be Stars. 2004, AJ, 127, 1682

24. Mikailov, Kh.M., Khalilov, V.M., Alekberov, I.A. Echelle-spectrometer of Kassegren focus of the two-meter telescope of the Shamakhy Astrophysical Observatory. 2005, Circular ShAO 109, 21

MWC361 ULDUZUNUN ŞÜALANMA SPEKTRİNİN SAKİT HALI

N. Z. İsmayılov, O. V. Xəlilov, S. Ə. Alışov

N.Tusi adına Şamaxı Astrofizika Rəsədxanası,
Azərbaycan Milli Elmlər Akademiyası, Şamaxı rayonu, Azərbaycan

Be Herbig tipli MWC 361 spektral qoşa ulduzunun spektral tədqiqinin nəticələri verilmişdir. Müşahidə fazaları sistemin şüa sürəti əyrisinin minimum fazalarına uyğun gəlir. Hidrogenin Hα və Hβ şüalanma xətləri aşağı səviyyəli şüalanma səviyyəsi göstərir. Ulduzun spektrində ilk dəfə DIB $\lambda\lambda$ 5780, 5797 Å diffuz ulduzlararası xətlər müşahidə olunmuşdur. 3 ay ərzində aparılmış müşahidələr göstərmişdir ki, hidrogenin, Si $\lambda\lambda$ 6347 6371 Å və [OI] $\lambda\lambda$ 6300, 6363 Å xətlərinin şüalanma komponentlərinin intensivliy nəzərə çarpacaq dərəcədə artmışdır.

Açar sözlər: AeBe Herbig tipli ulduzlar – Şüalanma spectri – Ulduzətrafı mühit – Dəyişkənlik – MWC 361

PECULIARITIES OF LINE VARIABILITY IN THE SPECTRUM OF κ CAS. I. PHOTOSPHERIC AND WIND LINES HeI

S. N. Gulahmadova [a], ***D. M. Kuli-Zade*** [a], ***A. Kh. Rzayev*** [b,c*]

[a] *Baku State University, Baku, Azerbaijan*

[b] *Shamakhy Astrophysical Observatory named after N.Tusi, Azerbaijan National Academy of Sciences, Shamakhy region, Azerbaijan*

[c] *Special Astrophysical Observatory, Russian Academy of Sciences, Nizhnij Arkhyz, Russia*

Temporal variations of radial velocities and profiles of the photospheric SiIII, OII, HeI, H_{10} - Hδ and wind HeI λ5875, 6678 lines were investigated in the spectra κ Cas. Rapid variabilities ($P < 1$ day) of radial velocities and line profiles were not detected. Radial velocity variability of all studied lines is mainly caused by non-radial pulsations. In case of photospheric lines the quasi-periodic variations were found for radial velocity variability. For wind lines HeI λ5875, 6678, patterns of temporal variability of radial velocity differ from each other and photospheric lines. Gamma-velocities and amplitudes of radial velocity variability were defined for them. The amplitude of spectrophotometric parameters and radial velocity variations, as well as rate of expansion increases from lower to upper layers of the atmosphere. Emission components are superimposed on line profiles correspondingly at positions of about -135 ± 10.0, -20 ± 20 and 135 ± 10.0 km s^{-1}. They are more obviously seen in the wind lines, but their traces are visible in all photoshperic lines. Such a pattern and character of the variability of all the line profiles in the spectrum of κ Cas show that it is a supergiant which shows the Be phenomenon.

Keywords: Supergiant-stars – Pulsation – Individual – κ Cas

1. INTRODUCTION

Despite its high brightness $V = 4^m.17$ [3] κ Cas was poorly investigated spectroscopically. These studies were conducted using a photographic method and

* E-mail: abid@sao.ru

have an informative character. Luud and Nugis [6] noted the variability of line intensity in the spectrum of κ Cas. Hutchings [2] found out that spectrum of a star isn't similar to a normal spectrum of a supergiant. On (the) line profile(s) of Hβ and Hα sharp, strong and pecular emission component is observed. Rosendal and Wegner [7] discovered that the equivalent width of strong lines changes almost twice. Walborn [13] classified κ Cas as a "carbon rich" star and gave it spectral class BC0.7 Ia. On the basis of studies of UV spectrum Searle et al. [11] defined κ Cas as a nitrogen weak star, rather than carbon rich. In the works of Ryans et al. [8], Simón-Díaz and Herrero [12] rotation velocity of a star which was about $v \sin i = 60\,\mathrm{km\,s^{-1}}$ was defined. Evolutionary parameters of the star were determined in the works of Crowther et al. [1] and Searle et al. [11]. In these works the parameters of T_{eff}, $R/R_\odot$ and $M/M_\odot$ differ and make 21500 K, 41.4 $R_\odot$, 40 $M_\odot$ and 23500 K, 33 $R_\odot$, 33 $M_\odot$. The photometric variability was investigated in the works of Koen and Eyer [3] and Lefèvre et al. [4] according to Hipparcos. The brightness variability with the period of $P = 2^d.647$ and amplitude of about $0^m.068$ was found. The radial velocity and line profile variability in time was not studied. In this paper temporal variability of radial velocities and line profiles of all photosheric and wind lines HeI λ 5875, 6678 Å were studied in the spectrum of supergiant κ Cas based on echelle-CCD spectra obtained during 36 nights.

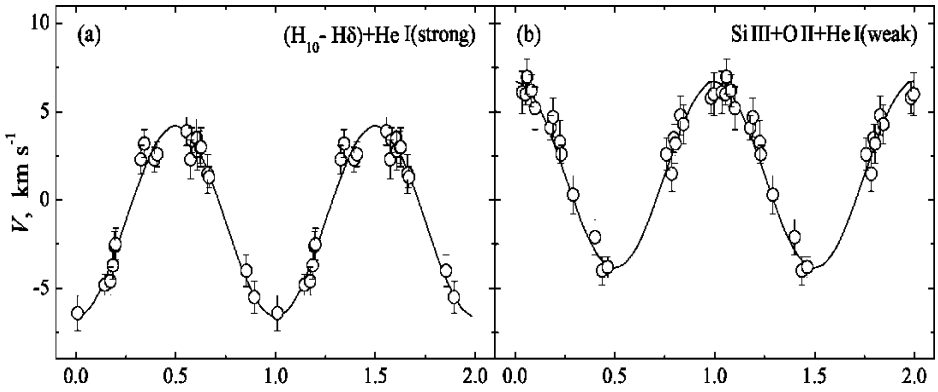

Fig. 1. Phase curves of radial velocities for the group of lines H_{10}–$H\delta$+HeI(strong) and SiIII+OII+HeI(weak). Curves were plotted according to the parameters: (a) $P = 4.16 \pm 0^d.05$, $V_\gamma = -1.5 \pm 0.5\,\mathrm{km\,s^{-1}}$; (b) $P = 4.60 \pm 0^d.08$, $V_\gamma = 1.5 \pm 0.5\,\mathrm{km\,s^{-1}}$. Initial phase JD_a = 2451452.38, amplitudes $A = 10.0 \pm 0.5\,\mathrm{km\,s^{-1}}$.

2. OBSERVATIONS AND MEASUREMENTS

Spectroscopic observations of κ Cas were carried out with the 2-m Terskol (Russia) telescope from August 31 to October 7, 1999. For this period 29 coude echelle spectra were obtained. 25 of them - for the period of 11 consecutive Julian dates ($JD_0 = 2451400 + 48 - 58$). The spectra were acquired with the resolution of $R = 45000$, and signal to noise ratio $80 \leq S/N \leq 600$ covering the spectral range of λ3600–11000 Å. To study rapid variability of line profiles and radial velocities in time 4, 4 and 5 spectra were obtained for three nights JD_0 + 52, 54 and 58, correspondingly. Exposure time for these spectra was $t_{exp} = 5 - 10$ min, an interval between exposures made $0.5 \leq \Delta T \leq 20$ hours. Over the nights JD_0 + 53, 55, 57 two spectra were obtained with $t_{exp} = 5$ min and $1.0 \leq \Delta T \leq 4$ hours. In these dates JD_0 + 22, 23, 48, 49, 50 duration of exposures was 30, 15, 60, 45 and 30 min, correspondingly, two spectra which were averaged for each night, were obtained.

Processing of echelle images was conducted by a standard method using software packages of DECH95[1)] and ESO MIDAS. Results of processing were identical. Measurement of positional and spectrophotometric parameters (equivalent width, central intensity and FWHM) of lines was performed using the software package of DECH20[1]. Measurement errors of spectrophotometric parameters were controlled on interstellar (IS) lines and DIB. The average value and mean-square deviation from the average for IS lines NaI λ5895 Å are $W_\lambda = 0.501 \pm 0.005$ Å, $r_0 = 0.028 \pm 0.002$, and for DIB λ5780 Å $W_\lambda = 0.287 \pm 0.01$ Å, $r_0 = 0.867 \pm 0.003$.

For calibration of the wavelength scale we obtained the spectrum of the Moon. The zero point of the radial velocities scale was established by telluric lines H_2O and O_2. Measurement errors for 60 telluric lines didn't exceed $|0.1| \pm 0.1$ km s^{-1}. Systematic measurement errors of radial velocities of stellar lines were also controlled by IS lines and DIB. The root-mean-square error from the average for NaI λ5895 Å and DIB λ5780 Å made -16.1 ± 0.4 and -7.2 ± 0.6 km s^{-1}, correspondingly. Measurement errors for the groups of lines OII, HeI, SiIII and single lines HeI λ5875, 6678 Å didn't exceed |1.5| and |2.0| km s^{-1}, respectively.

3. VARIATION OF RADIAL VELOCITIES AND LINE PROFILES

In our spectra of κ Cas in the above spectral range, about 300 lines are observed. Most of them, except lines HeI and hydrogen, have a weak intensity, and the relation S/N strongly differs for various regions of spectra. Therefore, for reliability of the results the lines were selected as follows: the lines were in

[1)] http://www.gazinur.com

the region of the spectrum, where $S/N \geq 150$, central depths of the lines were $R_0 = 1{-}r_0 \geq 0.15$. Thus, for investigations the lines of hydrogen were selected from H_{10} to Hδ, 12 lines HeI, two of them are wind lines HeI λ 5875, 6678 Å, four of them are designated as 'strong' ($R_0 = 1{-}r_0 \geq 0.27$) lines HeI λ 3819, 4026, 4471, 4921 Å, but the rest are designated as 'weak' ($0.15 \leq R_0 \leq 0.25$) lines HeI λ 3964, 4143, 4387, 4713, 5015 and 7065 Å, four lines OII (λ 4319, 4349, 4366, 4661 Å) and SiIII (λ 4552, 4567, 4574, 5739 Å). Wavelengths of lines were taken from Rzaev [10] to measure radial velocities.

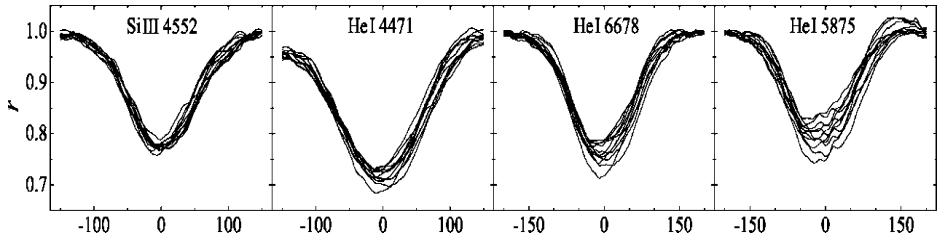

Fig. 2. Observed line profiles in the spectrum of κ Cas during our observations. Profiles obtained overnight, were averaged.

3.1. Radial velocity variability

We calculated Rosseland depths of line formations in the κ Cas atmosphere to study the stratification of radial velocity in the atmosphere. At the photosphere level $\log \tau_\lambda = 0$ was taken, this parameter takes a negative value for the layers of atmosphere and its absolute value increases to the upper layers of atmosphere. For all studied lines this parameter was defined at the level of half of their intensity. According to the ($\log \tau_\lambda$) values we conditionally divided the lines into three categories. Photospheric lines (lines SiIII, OII and weak lines HeI), strong photospheric lines (lines of hydrogen from H_{10} to Hδ and strong lines HeI) and wind lines (HeI λ 6678 and 5875 Å) respectively formed in 'lower', 'intermediate' and 'upper' layers of atmosphere. For these three categories of lines the average value of $\log \tau_\lambda$ was about -0.035 ± 0.01, -0.06 ± 0.012 and -0.098 ± 0.013, correspondingly. Analysis showed that for the lines specified above the patterns of the temporal variability of radial velocities were identical. These lines were respectively combined in the group of SiIII + OII + HeI(weak) and H_{10} - Hδ + HeI(strong). The patterns of the radial velocity variability showed periodic changes within 36 JD. The search for possible periods (or quasi-periods) of the temporal radial velocity variability for these groups of lines was carried out with the harmonic analysis [9]. Our investigations showed that rapid radial velocity

variability in time (P < 1day) is not detected. The observed variations of line profiles and radial velocities overnight reflect the variation on large time-scales. But in the course of searching for all groups of lines the radial velocities obtained for one JD weren't averaged. For 36 days within determination accuracy, the amplitude of radial velocity variability in time was identical for all photospheric lines: $A = 10.0 \pm 0.5\,\mathrm{km}\,s^{-1}$. The value of quasi-period (obtained with good significance value) is about $P = 4.16 \pm 0.05$ and 4.60 ± 0.08 days for groups of lines H_{10}–Hδ + HeI(strong) and SiIII + OII + HeI(weak), correspondingly. But gamma-velocity, V_γ for these groups of lines differs and makes about -1.5 ± 0.5 and $1.5 \pm 0.5\,\mathrm{km}\,s^{-1}$, respectively. Phase curves of radial velocities for these line groups are represented in Fig. 1. For wind lines HeI λ 5875, 6678 Å the pattern and nature of the temporal radial velocity variations differ from each other and photospheric lines. Several values of quasi–periods with small significance values were obtained for them within 36 JD. But V_γ and amplitude of the radial velocity variations were defined -2.0 ± 0.7 and $-8.0 \pm 1.0\,\mathrm{km}\,s^{-1}$, 13.0 ± 1.2 and $18 \pm 1.5\,\mathrm{km}\,s^{-1}$ respectively for lines HeI λ 6678 and 5875 Å. Therefore, the amplitude of the radial velocity variations and expansion velocity increase from lower layers to upper layers of the atmosphere. Double digits correspond to two last whole digits of the time of obtaining the spectra.

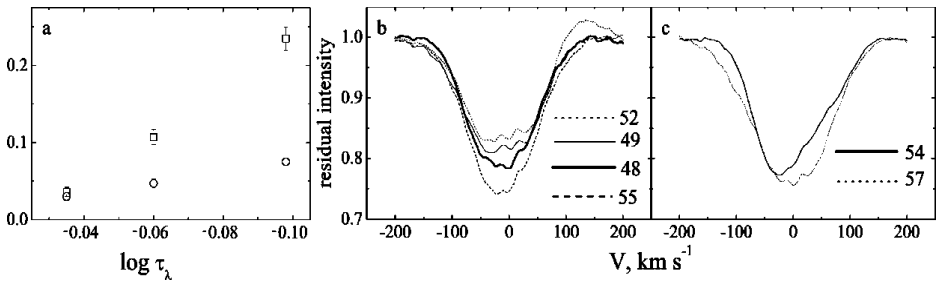

Fig. 3. (a) Variability amplitude $\Delta W\lambda$ (squares) and ΔR_0 (circles) for different groups of lines depending on the formation depth of these groups in stellar atmosphere. Horizontal axis is specially marked in reverse order to show the direction to upper layers of atmosphere. (b,c). Comparison of line profiles HeI λ 5875 Å. Double digits correspond to two last-whole-digits of the JD of obtaining the spectra. See the text for details.

3.2. Line Profile Variability

Measurements of spectrophotometric parameters of lines showed that the rapid variation of line profiles in time (P < 1 days) is not observed. The profiles obtained during one JD were averaged. Examples of the SiIII λ 4552 Å, HeI λ 4471, 6678

and 5875 Å line profiles are represented in Fig. 2. Both positional and spectrophotometric parameters of lines change for 36 days. Variations of spectrophotometric parameters of lines look more clearly at transition from photospheric lines to wind lines (Fig. 2). Fig. 3a shows variability amplitudes of equivalent widths, W_λ and central depths of lines, $R_0 = 1–r_0$ (over their maximum and minimum values) for photospheric and wind lines depending on the depth of their formation in stellar atmosphere. It is apparent that variability amplitude increases at transition from photospheric lines to wind lines (Fig. 3a).

Comparison of line profiles showed that the observed variations: blue – and red – shifted profiles, maximum and minimum values of central residual intensity of absorption, strengthening and decrease of emission intensity (or a trace) in blue and red wing of lines, etc. occur identically for all the studied lines. The pattern and trend of variability are similar for all studied lines, thus, for analysis we chose the line where these variations are most obvious. Fig. 3bc shows the comparison of (the HeI $\lambda\,5875\,$Å) line profiles. Double digits correspond to two last-whole-digits of the JD of obtaining the spectra.

Comparison of line profiles $JD_0 + 48$ and $JD_0 + 49$ shows that the emission at a position of $-20\,\mathrm{km\,s^{-1}}$ extending for $-80 \div 40\,\mathrm{km\,s^{-1}}$ is superimposed over the central part of absorption. There are no variations in the red wing, and the blue wing becomes gently sloping due to the reduction of intensity of blue-shift emission at the position $-135 \pm 15.0\,\mathrm{km\,s^{-1}}$. Further, up to $JD_0 + 52$ intensity of the central emission increases and then reduction of its intensity is observed. This continues up to $JD_0 + 55$ when the most intensive absorption is recorded. Then up to $JD_0 + 58$ intensity of the central emission strengthens again. In the night $JD_0 + 52$ red-shift emission appears in the red wing at the position about $135 \pm 10.0\,\mathrm{km\,s^{-1}}$ (Fig. 3b), and the next night $JD_0 + 53$ emission in the red wing is not almost obvious. In the dates of $JD_0 + 53$ and $JD_0 + 54$ in the blue wing blue shift emission appears at the position $-135 \pm 10.0\,\mathrm{km\,s^{-1}}$ (Fig. 3c). In the night of $JD_0 + 57$ the widest line was recorded, i.e. traces of emission on the wings 'have almost disappeared'.

Therefore, the variability of line profiles is also caused by appearances and 'disappearances' of emissions which are superimposed on the line profiles at three positions (Fig. 3bc). Blue-shifted, central and red-shifted emissions are at positions of about -135 ± 15.0, -20 ± 30 and $135 \pm 10.0\,\mathrm{km\,s^{-1}}$, correspondingly.

4. RESULTS AND CONCLUSIONS

Thus, in the spectrum of the supergiant κ Cas the variability of radial velocities and profiles of the photospheric SiIII, OII, HeI, H_{10} – Hδ lines and wind HeI $\lambda\,5875$, 6678 Å lines are mainly caused by non-radial pulsations. Rapid vari-

ations, $P < 1$ days, of radial velocities and line profiles were not detected. In case of photospheric lines we found periodic variations of radial velocity in time. The variability amplitude of the radial velocity was similar for all photospheric lines: A = 10.0 ± 0.5 km s^{-1}. The quasi-period is about P = 4.16 ± 0.05 and 4.60 ± 0.08 days correspondingly for groups of lines H_{10}–Hδ+HeI(strong) and SiIII+OII+HeI(weak). V_γ -velocities for these groups of lines differ and are -1.5 ± 0.5 and 1.5 ± 0.5 km s^{-1}, correspondingly. The derived periods correspond to non-radial pulsations in g modes (Lovy et al. [5]). The value of the γ -velocity, found for photospheric lines SiIII+OII+HeI(weak) demonstrates that the projection of radial velocity of the stellar mass center is about 1.5 ± 0.5 km s^{-1}. For wind lines HeI λ 6678 and 5875 Å V_γ -velocities and amplitudes were determined about -2.0 ± 0.7 and -8.0 ± 1.0 km s^{-1}, 13.0 ± 1.2 and 18 ± 1.5 km s^{-1}, respectively.

Equivalent widths and central intensity of lines also change over time. Amplitude of variability of these spectrophotometric parameters and radial velocity, as well as expansion velocity increase from lower to upper layers of atmosphere.

The variability of line profile is also caused by appearances and 'disappearances' of emissions which are superimposed on line profiles from three positions. Blue shifted, central and red shifted emission is at position about -135 ± 10.0, -20 ± 20 and 135 ± 10.0 km s^{-1}. These emissions are observed more explicitly on strong photospheric and wind lines, but their traces are obvious on all photospheric lines. Such a pattern and character of the variability of all the line profiles in the spectrum of κ Cas show that it is a supergiant which shows the Be phenomenon.

ACKNOWLEDGMENTS

Authors are very grateful to V.V.Shimansky for calculation of formation depths of lines in the atmosphere of κ Cas.

REFERENCES

1. Crowther, P.A., Lennon, D.J., Walborn, N.R. Physical parameters and wind properties of galactic early B supergiants. 2006, A&A, 446, 279

2. Hutchings, J.B. Expanding atmospheres in OB supergiants - IV. 1970, MNRAS, 147, 161

3. Koen, C., Eyer, L. New periodic variables from the Hipparcos epoch photometry. 2002, MNRAS, 331, 45

4. Lefèvre, L., Marchenko, S.V., Moffat, A.F.G., et al. A systematic study of variability among OB-stars based on HIPPARCOS photometry. 2009, A&A, 507, 1141

5. Lovy, D., Maeder, A., Noels, A. & Gabriel, M. Supergiant variability - Theoretical pulsation periods and comparison with observations. 1984, A&A, 133, 307

6. Luud, L. & Nugis, T. On the atmosphere of supergiant κ Cas. 1967, Pub. Tartu Astroph. Obs., 36, 183

7. Rosendhal, J.D. & Wegner, G. Spectrum Variations in A-Type Supergiants. 1970, ApJ, 162, 547

8. Ryans, R.S.I. , Dufton, P.L., Rolleston, W.R.J, et al. Macroturbulent and rotational broadening in the spectra of B-type supergiants. 2002, MNRAS, 336, 577

9. Rzaev, A.Kh., Hasanova, L.T., Yushkin, M.V., Mikailov, Kh.M. Nonstationarity of the atmosphere of α Cyg: II. Variability of the ion and Hβ line profiles. 2007, Astrophysical Bulletin, 62, 52

10. Rzaev, A.Kh. Investigation of Atmosphere Nonstationarity in the Supergiant 55 Cyg.I. Temporal Line Profile Variability. 2012, Astrophysical Bulletin, 67, 245

11. Searle, S.C., Prinja, R.K., Massa, D., et al. Quantitative studies of the optical and UV spectra of Galactic early B supergiants*I. Fundamental parameters 2008, A&A, 481, 777

12. Simón-Díaz, S., Herrero, A. Fourier method of determining the rotational velocities in OB stars. 2007, A&A, 468, 1063

13. Walborn, N.R. Spectral classification of OB stars in both hemispheres and the absolute-magnitude calibration. 1972, AJ, 77, 312

κ CAS ULDUZUNUN SPEKTRİNDƏ XƏTLƏRİN DƏYİŞKƏNLİYİNİN ƏLAMƏTLƏRİ. I. FOTOSFER VƏ HeI KÜLƏK XƏTLƏRİ

S. N. Güləhmədova [a], ***C. M. Qulu-Zadə*** [a], ***A. X. Rzaev*** [b,c]

[a] *Bakı Dövlət Universiteti, Bakı, Azərbaycan*
[b] *N.Tusi adına Şamaxı Astrofizika Rəsədxanası, Azərbaycan Milli Elmlər Akademiyası, Şamaxı rayonu, Azərbaycan*
[c] *Xüsusi Astrofizika Rəsədxanası, Rusiya Elmlər Akademiyası, Nijniy Arxız, Rusiya*

κ Cas ulduzunun spektrində Si III, OII, HeI, H10-Hδ fotosfer və HeI λ 5875, 6678 külək xətlərinin şüa sürətlərinin və profillərinin zamandan asılı olaraq dəyişkənliyi tədqiq olunmuşdur. Şüa sürətlərinin və profillərin P$<$1 gun zaman intervalında dəyişkənliyi aşkar olunmamışdır. Bütün tədqiq olunan xətlərin şüa sürətlərinin dəyişkənliyi qeyri-radial pulsasiya hərəkətləri ilə əlaqədardır. Fotosfer xətlərinin şüa sürətləri üçün kvazi-periodik dəyişkənlik tapılmışdır. HeI λ 5875, 6678 külək xətlərinin zamandan asılı olaraq dəyışkənlik əyriləri həm bir-birlərindən, həm də fotosfer xətlərindən fərqlənirlər. Bu xətlər üçün şüa sürətinin zamandan asılı olaraq dəyişməsinin gamma-sürəti və amplitudası tapılmışdır. Xətlərin spektrofotometrik parametrlərinin və şüa sürətlərinin dəyişmə amplitudası, həmçinin bu xətlərin yarandığı qatların genişlənmə sürəti atmosferin aşağı qatlarından yuxarı qatlarına doğru artır. Tədqig olunan bütün xətlərin üzərinə şüa sürətinin -135$\pm$10, -20$\pm$20, 135$\pm$10 km s^{-1} qiymətlərində emissiya komponentləri əlavə olunur. Emissiya xətlərində bu əlavə emissiya komponentləri aşkar şəkildə görünür, amma onların zəif izləri fotosfer xətlərində də müşahidə olunur. Xətlərin spektrofotometrik parametrlərinin və şüa sürətlərinin zamandan asılı olarag dəyişmə nümunələri və xüsusiyyətləri onu göstərir ki, κ Cas ulduzu Be fenomeni göstərən ifrat nəhəng ulduzdur.

Açar sözlər: İfrat nəhəng ulduzlar – Pulsasiya – κ Cas

MAIN SEQUENCE CHEMICALLY PECULIAR MAGNETIC STARS

S. G. Aliyev*

Shamakhy Astrophysical Observatory named after N.Tusi,
Azerbaijan National Academy of Sciences, Shamakhy region, Azerbaijan

In this paper the first part of a survey dedicated to the magnetic chemically peculiar (CP) stars, which are part of the general class (B0-F0) CP - main sequence stars, is presented. The main characteristics and classification of CP-stars are presented. The classification of Preston (1971), where chemically peculiar stars are divided into following groups: Am/Fm, λ Boo, Ap/Bp, Hg-Mn, He variable stars. According to scientific literature frequency of occurrence of CR-stars is about 15-20% among main sequence stars of spectral classes of BO – FO. The rotation periods of the most CP stars are within 0,5 - 100 days, however, there is also a small group of objects with particularly long variability periods. The chemical composition of the atmospheres of CP stars of various types is considered. Various mechanisms contributing in the appearance of chemical anomalies of inhomogeneities on the surface of CP-stars are shown. The preference is given to the hypothesis of selective diffusion of atoms under conditions of stability of the atmosphere of the considered stars.

Keywords: Chemically peculiar stars – Magnetic fields

1. INTRODUCTION

Magnetism as an integral part of matter is a widespread phenomenon in our Galaxy and beyond its limits. Magnetic field in the universe is ubiquitous and to some extent defines many physical processes or has a noticeable role in them. It has essential values in generation of different active formations, flares, bursts and many other nonstationary behaviors of space objects, including in our Solar system. Magnetic fields are observed in stars, galaxies and in interstellar space, they have various scales, intensities, configurations and lifetime. The study of the nature of magnetic field, generation and maintenance of space magnetic fields, as well as its roles in evolution of stars and the Galaxy is one of the most important

* E-mail: sabirshao5@gmail.com

directions of studies in modern astrophysics. Practically, magnetic field (Be) at observations of celestial objects is weak due to which it is hard to measure and estimate its size. Only in certain cases magnetic fields (magnetic white dwarfs of $Be \approx 10^2$G, pulsars of Be$\approx 10^{10}$ G, sunspots of Be $\approx 4 \times 10^3$ G, magnetic CP - stars $Be \geq 3 \times 10^4$ G), are measured more reliably. In these objects there is a possibility to study in detail physics of plasma in powerful magnetic fields, therefore, the role of magnetic field in formation of active occurrences in the Sun.

Magnetic field on the Sun has been first discovered in 1908 by G. Hale [1]. He could measure Zeeman splitting of lines in the spectrum of sunspots, cold formations existing for several months and occupying a small part of the Sun's surface. Magnetic field intensity in sunspots makes about 1-4 kG due to which it was measured easily. Besides, bright sunlight allows using spectrographs with high dispersion. The general magnetic field of the Sun as a star, apparently, is dipolar and its intensity makes only several gauss. Therefore it was impossible to find it due to insufficient sensitivity of the applied methods.

In 1947 H. Babcock developed the complex photoelectric solar magnetograph to measure a weak magnetic field [2]. He has developed and prepared the differential analyzer for circular polarization - the optical layout of which (a quarter wave - $\lambda/4$ Iceland spar) is still used nowadays. The principle of this technique consists in the following. The spectrograph builds the image of a stellar spectrum and some site of the Sun. Using the analyzer two opposite circularly polarized spectra are registered on a photo plate at the same time. Good rate accuracy for determining shifts between the left and right sigma – components of lines seen separately in each polarization can be achieved using the high resolution spectrograph. By this technique Babcock could discover a magnetic field in the star 78 Vir with abnormal lines of various elements [3]. As it is known [4] in uniform magnetic field Bp left- and right-hand circular polarized sigma (s) components of Zeeman triplet are shifted to the center of a line on a distance

$$\Delta\lambda = 4.67 \times 10^{-13} Z \lambda^2 Bp \qquad (1)$$

where Z – corresponding Lande factor of a line. Linearly polarized p - components are arranged symmetrically in the center of the line. Babcock's technique allows measuring the field if it has a noticeable longitudinal component (see below).

It is interesting that about 100 years ago, when carrying out a classification for HD Catalogue by E. Pickering, Antonia Maury found out that A-type star "Cor Caroli" (α^2 - Canes Venatici) had unusual strong lines [7]. When other A-type stars with anomalous spectra (lines) were discovered, they were named Ap (A-Peculiar) or α^2CVn stars. It appeared that chemical anomalies are also observed in some stars of spectral type B. In this regard these stars are generally called Ap/Bp stars. Stars with strong magnetic field located on top of the main

sequence have a number of interesting features. The most general features are: anomalies of chemical composition of the atmospheres and smaller axial rotations [5–9]. Such stars were called magnetic Ap - stars. These stars are bright enough that allows performing very detailed and high-precision researches of their spectra on large telescopes. The present work mainly deals with these stars.

The history showed that Babcock successfully selected objects to search a star magnetism only in Ap and Bp- stars. It was impossible to discover magnetic fields with complex structure (solar type) using photographic equipment, which existed in those days. Chemically peculiar (CP) stars are very convenient objects for researches of space magnetism. Magnetic field has a stabilizing role in CP-stars due to which favorable conditions are created for the operation of diffusion mechanism. According to [10] with the help of diffusion mechanism observed spots and other anomalies of chemical composition can be created for millions of years [11].

In the present work the research results of structures, chemical composition of the atmospheres, spectral variability of chemically peculiar (CP) stars of all types of peculiarities, as well as physical parameters (rotation, radii, masses, luminosity, duality and others) of these stars are analyzed.

Till the end of the XX century several good survey articles which have not been outdated partially or entirely today and devoted to a separate aspect of the study of magnetic chemical peculiar stars have been published. These works are [3–5] the fundamental monographs of Wolff [6], Preston [12], Romaniuk [7]. We will refer to these surveys further along with the original publications. In the present part of the survey the main attention is given, mainly, to new methods and results of the study of magnetic CP-stars.

Detailed complex - magnetic, spectral and photometric researches of magnetic SR-stars show that magnetic chemically peculiar stars are part of more general class (BO-F5) of main sequence chemically peculiar stars (CP) on Hertzsprung–Russell diagram. Strong general magnetic fields are discovered only in chemically peculiar stars which are located in the range of BO-F0. Therefore it is expedient and easier to give the description of general features of all CR- stars as a whole. Besides, the comparison of this group can lead to the detection of a number of peculiar features and their connection with a magnetic field.

Among various distinctive features of chemically peculiar stars allowing to allocate these abnormal objects from all stars in the spectral range of B0-F0, the most general features are the followings: the powerful magnetic field in a star, abnormally strong spectral lines of a great number of chemical (peculiar) elements (Si, Mn, Cr, Sr, Hg, P and rare-earth - Eu, Ce, Sm, Nd, Gd, etc.) and low (2-4 times) velocities of axial rotation [9, 14, 16].

Photometric and spectral variability and a number of other signs of CP-stars can be considered as derivative (secondary) signs. The intensity of those and other

peculiar effects depends on the value and geometry of a magnetic field, effective temperature of a star, type of peculiarity, mutual arrangement of axial rotation, magnetic axis of a star and orientation of these axes relative to the observer (effect of projection Sin i) [13]. Besides magnetic chemically peculiar (MCP) stars there are other CP-stars such as metal Am/Fm, mercury - manganese (Hg-Mn), etc. The fact that strong general magnetic fields are found only in stars which have anomalies in the chemical composition - a chemical peculiarity (CR) is of special interest. Results of spectral observations indicate a unique strong magnetic field coupling of a star with chemical anomaly, in the form of strong (more than 1.5 dex) anomalies of chemical composition. However not every chemically peculiar star has a strong magnetic field. The direct connection of a magnetic field with strong anomalies of the chemical composition has not been established yet. Therefore the researches of chemically peculiar stars with a strong magnetic field are of special interest in terms of understanding the mechanisms of origin of these uncommon occurrences.

Measurements and research of magnetic fields of chemically peculiar stars gives allows revealing various laws in a difficult interaction process of plasma and magnetic field. Despite nearly century-old history of studies of magnetic CP-stars, there are still a number of very important unsolved problems. The problem of origin of various types of anomaly of the chemical composition, origin of large-scale magnetic fields and loss mechanisms of angular momentum with these stars has not been solved completely [15, 16]. The most developed two competing hypotheses on origin of a field are: 1) in convective core of MCR-stars the dynamo mechanism operates, and the field generated there is brought on a surface of a star and becomes observable; 2) magnetic field is relic, it was formed together with a star with abnormal chemical compositions. But it is impossible to accept these hypotheses as both hypotheses have their own shortcomings and in most cases don't conform to the observation data [3, 4, 7].

Periodic intensity variations of spectral lines are related to uneven distribution of elements on a surface [18]. The observations available up to now indicate unambiguous connection of a strong regular magnetic field of stars with peculiarity in the form of strong anomalies of the chemical composition. The nature of this connection - whether magnetic field is a reason of anomalies in the chemical composition or magnetic field has not been established yet and chemical anomalies occur due to the action of some mechanism [3–5].

To explain a chemical anomaly in the atmospheres of magnetic stars various mechanisms and hypotheses were suggested: 1) Nuclear reactions on surfaces and in stellar environment. 2) Accretion of interstellar abnormal chemical gas on a star. 3) Diffusion separation of elements under the gravity force and radiation pressure, etc. All these and other suggested mechanisms were discussed in detail

in literature [4–6] where it was shown that none of these mechanisms can explain the origin of a chemical anomaly in CP-stars. There is one more unsolved problem – slow axial rotation of MCP - stars. It is known that on average rotation velocity of magnetic stars are 2-4 times lower than rotation velocity of normal stars of similar spectral classes and luminosity [7, 13, 15]. The average value of projected equatorial velocity to line of sight (Vsini) for normal stars it is 177 km/s, for peculiar stars – 52 km/s. It has not been defined yet that why and at which stage of evolution peculiar stars lose the great part of their angular momentum [14–16].

2. SEPARATION AND CLASSIFICATION OF CP-STARS

CP - star can be easily distinguished from normal stars by spectrum. The main observed signs: except the lines of hydrogen the lines of metals and rare earth elements are strengthened, and the lines of calcium are weakened; anomalies are visible even at low dispersive photographic spectra in visual inspection. Using this indication CP- stars were selected for compiling HD catalogue at the end of CIC century. Besides specified signs it was found that the amount of observed spectral lines in spectra of CP - stars is nearly 7-10 times more than those of normal stars with similar temperature [20].

A great number of works on researches of CP - stars have been published and many attempts were made to give the general classification of these stars. However, despite some general static laws observing specific spectral features of these stars are so high that it is unlikely to find two chemically similar stars. Other distinctive properties of CP – stars, in particular, wide and small depressions in their continuous spectra, the most noticeable of which are located in the range of about λ 14200 and λ 15200 ÅÅ, have been currently found [22, 23].

This allowed developing the photometric methods of separation of CP - stars [23]. Photoelectric photometry was effective in searching CP stars and their classification [24].

Though spectral and photometric characteristics of CP stars are very different, many attempts have been made to give the general classification of CP stars. Prior to the beginning of 1960 years of the last century spectral classification of CP stars was created approximately. The concept of quantitative degree (index) of a peculiarity has been first introduced by V.V. Leushin [25]. Subsequently in 1987 Kopylov [10] determined the quantitative indexes of a peculiarity (R) by the chosen lines of different elements SiII, MnII, CrII, SrII, and EuII, for 60 CP - stars. He studied the behavior of peculiarity (P) degree of along the temperature sequence.

Table 1. Classification of CP stars

Group. CP	Name of class	Classification criteria	Temprature interval K	Rotation (km/s)	Frequency of occurences (%)	Duality (%)	Spectra of classes
CP1	Metalline Am - stars	Weak CaII ScII Abundance of heavy metals	7000 - 10000	< 40	> 30	> 65	A5-F0
CP2	Magnetic Ap/Bp stars	Abundance of Si, Cr, Sr, Eu and other.	7500 - 20000	≤ 60	≈ 20	45	A5-F0
CP3	Hg-Mn stars	HgII 3984 Mn variable	10000 - 15000	Slow.	Norm.	<60	B6-B9
CP4	He-variable	He-weak P,Ga He-strong	13000 - 18000 18000 - 22000	100- 150	? ≥ 15	- -	B4-B6 B0-B3
	λBoo	Deficit of metals 0,5 dex, MG-Ni	9000 - 11000	≤ 20	?	?	B9-A2

According to the modern ideas CP star can be subdivided into two general groups: magnetic and non-magnetic [7]. Rather strong (Be $\geq$ several kG), ordered magnetic fields were measured at stars Ap/Bp in the spectral range of B0-FO. However, strong (Be^3 200 G) magnetic fields in different CP stars, such as Hg - Mn, Am/Fm, He-weak, and λ Boo type stars have not been found [26]. There are various systems of classification of CP stars based on the dependence of any peculiarities on physical and chemical parameters of these objects. For example, Jaschek and Egret [27] offered to divide CP - stars to the following groups: 1) stars with abnormal helium lines are divided into 3 subgroups; 1- with strong helium lines (He-r), 2- with weak helium lines (He-w), 3-with variable helium lines; 2) classical Ap stars are divided into 4 subgroups: 1 - Si λ 4200 and Si, 2 - Hg-Mn, 3 – Si +, 4 SrCrEu in different combinations; 5 – Am - stars, 6 - λ Boo type stars. Authors [27] state that stars with weak helium lines and Si λ 4200 type stars have some characteristics. There are also photometric classifications of CP stars that are based on the measurements of value of anomalies (depression) in distribution of energy in continuum spectrum. According to [28] CP stars are separated differently in various photometric systems. Apparently, such disparity shows our limited understanding of physics of peculiarity of CP stars as it was noted in [7].

Preston classification [12] in which all CP stars are subdivided into 4 groups depending on the type of peculiarity and temperature was widely used among published works: CP1 -Am/Fm stars with strong metal lines (the coldest Te=7000-10000k), CP2-magnetic Ap/Bp-stars (Te=7000-20000K), CP3-mercury-manganese (Hg-Mn) stars (Te=10000-15000K) and CP4-the hottest (1300-20000K) stars with abnormal helium lines. In our opinion Preston [12] classification is the most physical. Therefore in further statement we will follow this classification. Below we will present it considering some modifications [29] (see Table 1 in [7]), as well as with new data for CP stars obtained generally in 2000-2016.

3. STARS WITH STRONG METAL LINES AM/FM

According to the classification of Preston [12] CP1 group contains colder (7000-9000K) and less massive Am/Fm stars located in the range of spectral classes F5-A8. In the atmospheres of these stars there is a deficiency of Ca, Sc and abundance of Sr and lanthanides (Eu, Sm, etc.). Spectral and photometric variability were not found in these stars. However there are pulsing stars of δ Sct and δ Del with the same temperature and mass in the region of Hertzsprung–Russell diagram. It should be added that results of the subsequent researches have shown that in several Am/Fm stars (15 Vul, χ Ser and 68 Tau) photometric and spectral periodic variability typical for magnetic CP stars are observed [31,34]. Axial rotation velocities of these stars are small, as a rule, Vsin i $\leq$ 10 km/s. According to [32] the percentage of double among them is much more ($\geq$ 60%), than in normal stars (45%) of the same spectral classes. The duality of metallic-line stars complicates the exact definition of the chemical composition. Problems in defining the chemical composition of Am and other CP stars are discussed in detail in [11,26]. Effective temperatures of metallic-line stars have been more precisely determined by method of infrared flux [35].

The chemical composition was studied using different analysis methods of the atmospheres of many metallic-line stars [26]. It was determined that the composition of Cr, Ti, and Fe- are close to solar, light elements (Ca, Sc and others) are almost one degree lower than normal, the composition of heavy (La, Nd, Eu) and super-heavy elements (Os, Pm, U) are strengthened, by approximately 1-2 orders. The composition of 26 chemical elements is given in Lyubimkov's monograph [26]. It was determined that anomalies in the compositions of these elements grow as atomic number increases. The question on a magnetic field at metallic-line stars is still discussed. In the catalogue of Babcock [33] magnetic fields of two Am- stars ($Be \approx 400 \pm 40\%$ G in 68 Tau and 375 ± 35 G in 16 Ori) were shown. Kuvshinov, et al. [34] have found a variable magnetic field of 100 G order in Am – stars 15

Vul and 68 Tau on the photometric magnetometer. Authors [34] state about the detection of a magnetic field, on magnetic line broadening, about 2 kG in Am-star OPeg, but the structure of a field is complex. If the field of Am/Fm-stars exists, then it has a complex, nondipole configuration.

Boyarchuk, et al. [37] have found a correlation of content of vanadium with a rotation velocity - the more Vsini, the less anomaly of composition. High-precision measurements of 4 Stokes parameters with high spectral resolution are necessary to identify magnetic fields with possible complex structure in Am/Fm stars. Observations of circular polarization show that Am/Fm - stars have no large-scale longitudinal magnetic fields, while line broadening caused by the fields which have a complex nondipole structure [7], is observed.

4. MAGNETIC AP/BP STARS

Magnetic Ap/Bp stars are a part of more general class of main sequence CP stars on Hertzsprung–Russell diagram. According to the classification of Preston MCP stars were included into the second group (CP2) of stars. This is more extensive group and significantly differs from other CP stars as to its properties. They are detected almost in all ranges of spectral classes of CP stars B0-F0. Magnetic Ap/Bp stars were detected in clusters of different ages (log t = 6,4 - 8,7) [15]. Nearly 70 years have passed since the detection of the first magnetic star 78 Vir by Babcock [2]a. Presently it has been already found out that MCP stars have sharply expressed chemical inhomogeneous anomalies on their surfaces, the considerable spectral and photometric variability, slower rotation than in normal stars [9,14,16].

Changes like pulsations (instability of seismic character) are detected in some late spectral classes (A5-F0) of MCP stars [38,39]. Other properties distinguishing them from normal stars of the same spectral classes were also revealed [3,7,40]. In spectra of these stars strong lines of some (peculiar) elements, in particular Si, Cr, Sr, Mn, Fe, Eu, Nd, Gd, Ce, etc. are observed. Deficit of Ca, Sc and other light elements ($\mathcal{Z}$ <14) is detected. Overabundance of heavy elements (Pm, Os, U) about 2 - 4 dex was detected [41]. Brightness and color of MCP stars change periodically with a small amplitude [42–44] which correspond to the change of temperature 500-1500K [45,46].

The main distinctive peculiarity of magnetic stars is a strong regular, periodically varying magnetic fields of global character with value from hundreds of G to several tens of kG. Unlike the Sun general dipolar field of which does not surpass several Gauss like a star, magnetic stars have strong regular fields on all or a considerable part of a surface reaching 34 kG (HD 215441 star) [33]. These fields are detected in integrated stellar spectra (from all visible surfaces) by Zeeman

effect. Further [47,48] it was reported that they have detected an extraordinary (with a double wave) variability of magnetic field Be at HD37776 star which can be explained only in the assumption that quadrupolar component of its magnetic field is many times stronger than dipolar component. The longitudinal field of Be which varies with a rotation period phase (1.5387 days) within the ranges of 2000 to +2000 G was measured using hydrogen magnetometer. It has been proved by the best way of observations that this star has a strong quadrupolar field in order 60-70 kG [47].

The periods of variations of a magnetic field from 0,5 to 140 days are known by now, but most of the periods are concluded in the range from 2 to 20 days. Practically all magnetic Ap - stars are magnetic, photometric and spectral variable with the same period which is a period of stellar rotation. The variability of magnetic CP stars can be explained by oblique rotator model. The surface of these stars is inhomogeneous by their properties. In such model the magnetic axis, rotation axis and line of sight do not match with each other [3,7,49]. All subsequent numerous spectroscopic researches, measurements of magnetic fields and photometric variability confirm oblique rotator model [49–52].

However by oblique rotator it is impossible to explain short-term variability which is detected in cold SrCrEu stars. In late 1970s in [38,53,54] rapid pulsating, so-called ro - Ap - stars which pulsate with the periods from 6 to 16 min., with an amplitude up to 0,008 of stellar value have been detected. The wide review of ro-Ap stars till 2000 was provided in the work of Kurtz and others [53]. In this work it was noted that many of them have strong magnetic fields. More than 30 such objects have been currently detected. Pulsation of MCP stars and their interpretation will be considered in detail in the following works.

MCP stars occupy area of effective temperatures ranging from 7500-20000 K on Hertzsprung–Russell diagram. Calculations of model atmospheres of peculiar stars due to the strong absorption in lines caused by abnormal chemical composition have shown that the atmospheres of magnetic stars are similar to the atmosphere of a normal star with higher effective temperature [55–57]. In this regard new calibrations of effective temperatures were performed especially for peculiar stars which ensure a good temperature scale for magnetic stars [57–59].

Most of published works showed that almost all Ap - stars are slow rotators [3,14,60,61]. Slow rotation together with a magnetic field makes stellar atmosphere stable enough for separation processes of chemical elements. Here magnetic field only increases the stability of the atmosphere. If chemical anomalies are a consequence of slow rotation, then the question on the formation of chemical anomalies is closely connected with a question when Ap - star has begun rotating slowly. This question was explained thoroughly in the works [16,60–62].

5. MERCURY-MANGANESE STARS

According to the classification of Preston mercury- manganese stars belong to the third group (CP3) of stars which are located in the field of spectral classes AO-B8, i.e. in the range of temperatures 10 000-14000K. Important peculiarity of these sterrla atmospheres is overabundance of Hg and Mn lines. Their spectra are typical for strong lines of mercury, manganese, platinum, cobalt, chlorine, but helium lines are strongly weakened in spectra. Mn-Hg - stars like metal Am - stars don't show noticeable spectral and photometric variability [3]. The chemical composition was defined using Zeeman-Doppler imaging (Z-D) and model atmosphere [3, 26]. It was determined by Lyubimkov [26] that abundance of mercury is 4-5 order, and manganese - 1-3 order. It is noted that the growth of anomaly in the composition of elements with high atomic number of Hg-Mn stars is considerably less than atomic number of Am/Fm and Ap/Bp stars. These stars as magnetic Ap - stars rotate more slowly than normal stars.

The catalogue of Hg-Mn – stars which contains 110 objects, was compiled in the work [63]. More than 60% of these stars are included into the double systems [7]. These stars differ in smaller degree of peculiarity than classical magnetic Ap/ Bp-stars. Photometric variability was not detected in Hg-Mn stars and depression in a continuous spectrum of λ 5200 Å is very low. Signs of spottiness on a surface are not also detected in them. However, uneven distribution of mercury on a surface of two Hg-Mn stars, (HRII85 and HR8723) which are similar to α and star by the chemical composition, was detected in the work [64] of Kochukhov and etc. [65]. The spots on profiles of resonance HgII line λ 3984 Å showing variability of a profile for 2 days, has been detected in these stars. It is assumed that observed irregularities of mercury is a consequence of dynamic instability in chemical diffusion and are not connected with magnetic fields.

Dipolar magnetic field (Be $\geq$ 200G) is not observed in Hg-Mn stars, since mercury spots are an indirect argument in favor of a field at these objects. Basing to several works (for example, [7] and references to it), we may consider that strong (kG) dipolar magnetic field does not exist in the atmospheres of Hg-Mn stars. However the existence of strong field at Hg-Mn star HD22316, longitudinal component of which varies periodically and in a maximum exceeds 2 kG, has been confirmed with observations on the 6-m telescope of SAO RAS [7]. There are many references to the magnetic field as a reason of line broadening if it is assumed that there are kG fields with a complex structure (nondipole) in the atmosphere of Hg-Mn stars.

Many works were devoted to the analysis of the chemical composition of Hg-Mn stars [20,26,65]. One of the main works is the work [65] where the abundances of Hg, Mn, P, Sc, Cr, Eu in the atmospheres of two Hg-Mn stars - *alpha* and π^1Boo

were detected. This work belongs to the period when the chemical composition was defined using a traditional curve method of growth, therefore the results are not so reliable. In the late 80s CCD-matrixes were used to increase the accuracy of observations and definition of the chemical composition using Zeeman-Doppler mapping [3,66,67].

From the opinion on the lack of measurable magnetic longitudinal field, lack of noticeable spectral and photometric variability and behavior of the chemical composition we may state that Mn-Hg stars are the continuation towards higher temperatures of the sequence of Am-stars [7].

6. λ BOO TYPE STARS

λ Boo type stars belong to non-magnetic stars which have a spectral class between AO and Fo stars on hydrogen lines and KCaII. Weak lines of metals and MgII λ 448I Å lines which are used in most of star classifications are present in spectra of these stars. The group of these stars is absent in the classification [12]. The classical standard α Lyr (Vega) star belongs to this type. This star was accepted as a standard by the chemical composition and other parameters for a long period. Vega is not the only A-star of GP which have a general metal deficit. In a spectral class of AO a certain group of stars with similar chemical anomalies like in λ Boo is separated.

Classification peculiarities of a chemical composition of this type stars were given in the monograph of Lyubimkov [26]: 1) practically normal content of C, N, O; 2) deficit of a number of metals from Mg to Ni is about 0,5 dex. However, the results of subsequent researches [26] for these stars have shown that Fe deficit is stronger: [Fe/H] = -2,0; -1,8 and-1,3 respectively for λ Boo, 29 Cyg and p Ori. The content of C, N, O, and S was close to solar. The chemical composition of 15 stars of this type was defined by Sturenburg [68]. All chemical elements from Ca to Ba, except carbon, show a tendency to a deficit about 1,0 - 1,5 dex. According to [69] many λ Boo type objects are pulsing stars of δ Sct class as well.

However, these objects are not very old stars, metal deficit can be explained by the mechanism of gravitational diffusion assuming that weight loss with order velocity of about 10^{-13} mass of the Sun occurs per year. The second hypothesis – the reduction of metal content is a result of accretion on these stars of interstellar substance. Using the data of Hipparcos satellite absolute star values were detected and the evolutionary status of λ Boo type stars were determined [70]. As it is noted, metal deficit is detected in λ Boo type stars, and they rotate rapidly, the lines in their spectra are very weak and wide. Therefore the measurement of magnetic fields is almost impossible by the photographic way [71]. Bohlender and Landstreet [72] have published a big review of magnetic measurements of λ Boo

type stars. Authors note that longitudinal magnetic field was not detected on hydrogen lines in any of these objects. If these stars have a large-scale magnetic field, its longitudinal component does not exceed 200 - 300 G [7].

7. STARS WITH ABNORMAL He LINES

Stars with abnormal helium lines belong to the fourth group - CP4, according to Preston classification [12]. Effective temperatures (Te = 13000-25000K) and accelerations of gravity (log g = 4 – 4,5) correspond to main sequence B-stars. These stars consist of two subgroups: 1) colder stars of He - weak with weakened lines of helium in spectra; 2) hotter He-rich (or He-strong) with strong lines of helium. CP 4 stars have strong magnetic fields (see below), like in magnetic CP2 stars. The general survey for stars with abnormal lines of helium is given in the works [73–75]. There are no photometric criteria for He-r star which allow distinguishing them from normal stars of a spectral class B. According to [7,74] H-wk stars are divided into 3 subgroups: 1) phosphorus (P) gadolinium (Gd) stars which don't show photometric and spectral variability, 2) silicon (Si) stars, 3) SrTi –stars showing spectral and photometric variability. Stars from CP 4 rotate rapidly, average values of axial rotation ($\nu \sin i$) are in the range of 100-150 km/s. Rotation periods of these stars are 1 - 1,5 days [7]. The chemical composition of helium stars has been defined by Lyubimkov [26] in which it was determined that unlike CP - stars of other types, the growth of anomaly degree in contents with high atomic number of an element was not detected for helium stars. The work of Glagolevsky, et al. [74] presents the additional data of the impact of magnetic field on the content of helium at stars with strong helium lines.

Using Doppler - Zeeman mapping [75] inhomogeneity of the chemical composition of a surface of helium stars like in CP 2 stars was detected [76]. In the atmospheres of He-r stars the relation He/H reaches 70% [77]. Magnetic fields were detected for 12 stars with weak helium lines [78]. Bohlender, et al. [72] showed that He-r stars have three times more magnetic field intensity than CP-2 stars. The work [79] has studied the configuration of a magnetic field and its connection with distribution of chemical anomalies to surfaces of helium CP star of HD 37776 which has a strong quadrupole field of about 60-70 kG. Several massive stars with variable helium lines in which changes of magnetic field intensity cannot be described by displaced dipole were detected, i.e. there is a multi field of higher orders. These stars (HD 32633, HD 37776, HD 133880) are the hottest representatives of CP - stars and have the strongest (60-70 kG) magnetic fields. The works devoted to the study of a magnetic field of a unique HD 37776 star have been surveyed in detail by Romanyuk and others [79]. Authors of this work concluded that surface field of this star has a quadrupole configuration and reaches

more than 60 kG. In [78] it was found out that around stars with strong magnetic fields there are emission nebulae which can occur due to mass loss and rotation moment of these stars. Comparison of the data on distribution of surface chemical anomalies with not only values, and also with magnetic field configuration is of the greatest interest to understand physics of magnetic CP stars [79].

8. CONCLUSIONS

In this part of the survey the general properties of chemically peculiar (CP) stars which include magnetic Ap/Bp stars have been reviewed. Some general questions were explained partially or absolutely omitted, but herein early excellent surveys have been referred to [2–7]. A part from these questions, in particular, concerning magnetic CP stars will be reviewed in the following part (II) of this survey. Among aforesaid questions, one question is more interesting: how do magnetic CP-stars differ from nonmagnetic stars. The main individual characteristics and their anomalies in a chemical composition were explained for all reviewed nonmagnetic stars. The main peculiarities of magnetic Ap/Bp stars (unlike nonmagnetic) are the followings: 1) strong (kG) dipolar magnetic field; 2) sharp anomalies of a chemical composition of various elements; 3) spectral and photometric variability; 4) small axial rotation velocity (vsin i 70 km/s); 5) lack of double stars compared with normal stars of GP main-sequence.

Modification, improvement and enhancement of observation methods, their reduction and implementations of CCD-matrix permits to measure weak magnetic fields and to define the composition of different elements in stellar atmospheres with an accuracy of 0,2dex order. Doppler - Zeeman mapping (D-Z) of a surface of CP stars has been applied for brighter stars. Useful data on chemical composition of peculiar and normal stars are provided in the monograph of L.S. Lyubimkov [26]. The study of helium-variable stars in which strong quadrupole magnetic fields of about 60-70 kG order were detected, is of special interest. Perhaps, there are stars among non-magnetic CP-stars that have nondipole magnetic field with high configurations. In the second part of our survey we are planning to explain the main results of complex researches and study of a magnetic field configuration for magnetic Ap/Bp stars.

REFERENCES

1. Hale, G.E. Magnetic field of the spot on the Sun. 1908, ApJ, 28, 315

2. a) Babcock, H.W. Zeeman effect in stellar spectra. 1947, ApJ, 105, 105
b) Babcock, H.W. Remarks on stellar magnetism. 1947, PASP, 59, 112

3. Khokhlova, V.L. Magnetic stars. 1983, Results of science and technology book. Moscow, VINITI, 283

4. Pikelner S.B., Khokhlova V.L., Magnetic stars. 1972, Advan. in Phys. Sci., 107(3), 389

5. Khokhlova, V.L. α^2 Canes Venatici type stars. Eruptive stars. Moscow, 1970, 307

6. Wolff, S.C. The A-type stars: Problems and perspectives, Monograph series on Nonthermal Phenomena in stellar atmospheres, NASA, 1983, SP-463, Washington, D.C. 211

7. Romanyuk, I.I. Main sequence magnetic CP stars II physical parameters and chemical composition of atmosphere. 2007, Astrophys. Bull., 62, 72

8. Kopilov, I.M. Stellar rotation. 1995, Bull. of the Crimean Astrophys. Observ., 90, 14

9. North, P. Rotation of -Stars. 1984, A&A, 141, 328

10. Michoud, G., The astrophysical contex of diffusion in stars.1980, AJ, 85, 589

11. Khokhlova, V.L. Peculiarities of anomaly of the chemical composition of atmospheres of magnetic Ap - stars. 1976, Astron. Nachr., 297(5), 217

12. Preston, G.W. The chemically peculiar stars of the upper main science. 1974, ARA&A, 12, 257

13. Kopilov, I.M. Qualitative spectral indices of peculiarity of CP of the upper main science. 1987, Bull. of SAO, 24, 44

14. Klochkova, V.G. & Kopilov, I.M. On rotation velocity of CP stars. 1985. Astron. Rep., 62, 947

15. Klochkova, V.G., Kopilov, I.M. CP stars in the groups of various ages. 1966, Astron. Rep., 63, 240

16. Aliev, S.G. & Khalilov, V.M. The observed rotation peculiarities of magnetic CP stars. 2013, AAJ, 8(3), 52

17. Boyarchuk, A.A., Yefimov, Y.S., Stepanov, V.E. Magnetic amplification of absorption lines. 1960, Bull. of the Crimean Astrophys. Observ., 24, 52

18. Kolev D.Z. Magnetic intensification of lines in spectra of cold Ap - stars. 1977, Astron. Lett., 3(8), 363

19. Stibbs, D.W.N. A study of the spectrum and magnetic variable star HD125248. 1950, MNRAS, 110(4), 395

20. Aliev, S.G. Spectral study of magnetic CP-stars based on spottiness effect. PhD thesis. 2003, BSU, 170

21. Kodaira, K. Osawas peculiar star HD221568. 1969, ApJ, 157, 59

22. Glagolevskii, Y.V. Some results of the study of continuous spectra of magnetic and peculiar stars. 1966, AZh, 43, 73

23. Straizys, V., Zytkyavichus, V. Separation of AP stars in Vilnius photometrical system. 1977, Astron. Lett., 54, 5

24. Straizys, V. Multicolor stellar photometry. Vilnius, Mokslas, 1977, 305

25. Leushin, V.V. Qualitative study of peculiarity in spectra of Ap stars. 1971, Astrophys. Stud. (Bull. SAO), 3, 36

26. Lyubimkov, L.S. Chemical composition of stars: method and results of analysis. Odessa, Adtroprint, 1995, p.3-323

27. Jaschek, M., Egret D. Catalogue of Stellar Groups. Publ. Specialties. CDS. 1982, 4, 1

28. Faraggiana, R. Recent progress in CP star detection and classification. 1987, Ap&SS, 134 (2), 381

29. Kurtz, D.W. Rapidly oscillating magnetic Ap - stars. 1990, ARA&A, 28, 607

30. Savanov, I.S. Qualitative analysis of atmospheres of two "metalline" stars (68 Таи, cSer). 1983, Bull. of the Crimean Astrophys. Observ., 66, 139

31. Aliev, S.G. On spectral variability and physical conditions in atmosphere of Am star HD189849. 1991, Circular of ShAO, 89, 17

32. Abt, H.A. & Snowden, M. S. 1973, ApJS, 25(215), 137

33. Babcock, G.U. Magnetic fields of stars, Reports stellar atmosphere, under editorship of G.Grinstein. M. IL., 1963, 283

34. Kuvshinov, V.M., Hildebrandt, G., Schoneich, W. Bull. of the Crimean Astrophys. Observ., 1975, 53, 253

35. Blackwell, D.E. & Shallis, M.J. Effective temperatures for Am stars. 1977, MNRAS, 80, 177

36. Mathys G., Lanz T. The magnetic field of the Am- star O Pegasi. 1990, A&A, 230(1), 21

37. Boyarchuk, A.A. & Savanov, I.S. Upper Main Sequence Stars with Anomalous Abundances, IAU Coll. 1986, Crimea, Reidel, 90, 433

38. Kurtz, W. Metallicion and pulsation the marginal metallic line stars. 1978, ApJ, 221, 869

39. Aliev, S.G. & Ismailov, N.Z. Discovery of rapid variability of spectra of Ap star c Psc. 2000, Astron. Rep., 77, 834

40. Romanyuk, I.I., Kudryavtsev, D.O., Semenko, E.A. Magnetic fields in stellar rotation with strong and weak anomaly in distribution of energy in continuum. 2009, Astrophys. Bull.,64(3), 247

41. Aliev, S.G. Lines of heavy elements in the spectrum of magnetic Ap star HD 220825. 1981, Astron. Zh., 58, 355

42. Peterson, D.M. The photometry variability of Ap – stars. 1970, ApJ,161, 685

43. Schoneich, W. Photometric study of magnetic stars. Reports of Magnetic Ap – stars. Baku, Elm, 1975, 3

44. Preston, G.W. Characteristics of the magnetic stars. 1971, PASP, 83, 571

45. Provin, S.S. Variation in light of the spectrum variable 56 Aries. 1953, ApJ, 118(2), 281

46. Aliev, S.G. Determination of effective temperatures of magnetic stars based on inhomogeneity of atmosphere. 2010, Bull. of ANAS, 35(2), 173

47. Thompson, I.B. & Landstreet J.D. The extra ordinary magnetic variation of the helium-strong star HD37776, A quadruple field configuration. 1985, ApJ, 289, 1, L9

48. Romanyuk, I.I., Elkin V.G., Shtol V.G. Observation of four Stokes parameters in the continuum of He-rich star HD37776. Stellar magnetism, Proceedings of international meeting. Sankt- Petersburg, 1992, 57

49. Stibbs, D.W.N. A study of the spektrum and magnetic variable star HD 125248. 1950, MNRAS, 110, 395

50. Deutsch, A.J. Harmonic analysis of rigidly rotating Ap-stars. 1970, ApJ, 159, 985

51. Borra, E., Landstreet, J. The magnetic field of Ap-stars. 1980, ApJS, 42(3), 421

52. Schoneich, W. 23d Intern. Conf. On Astrophys. «Upper Main Sequence CP-stars, Liege, 1981, 235

53. Kurtz, D., Martinez P. The stellar pulsations. 2000, Balt Astron, 9, 253

54. Aliev, S.G. & Ismailov N.Z. Search for rapid variability of spectrum of Ap star g Equ. 2001, Phys., 7(1), 42

55. Muthsam H. Line blanketed model atmospheres of Ap-stars.II.Numerical rtzults. Astron. Astrophys. Suppl. Ser, 1979. V.35.P.107-109.

56. Muthsam, H. Line blanketed model atmospheres of Ap-stars. II Numerical rezults. 1979, A&AS, 35, 107

57. Muthsam, H. Line blanketed model atmospheres of Ap-stars. I. 1979, A&AS, 73, 159

58. Megessier, C. Effective temperatures and angular diameters of Ap-Bp Si stars and B and A normal stars. 1988, A&AS, 72, 551

59. Stepien, K. & Dominicsoc R. Effective temperatures of Ap stars. 1989, A&A, 219, 197

60. Wolff, S.C. Rotation velosities of magnetic Ap stars. 1981, ApJ, 244, 221

61. Ryabchikova, T.A. Magnetic Ap-stars; evolutionary status and anomaly of the chemical composition. Chemical evolution of stars and galaxy. Moscow, Kosmosinform, 1992, 108

62. Romanyuk, I.I. Upper main sequence magnetic CP stars Nijniy Arkhiz. 2004, Dr. of sciences thesis in phys.-math., 520

63. Schneider, H. A catalogue and bibliography of Mn-Hg stars. 1981, A&AS, 44, 137

64. Kochukhov, O., Piskunov, N., Sachkov, M. & Kudryavtsev D., 2005, A&A, 439, 1093

65. Khokhlova, V.L., Aliev, S.G., Rudenko, V.M. Study of spectra of peculiar manganese type Ap stars. 1969, Bull. of the Crimean Astrophys. Observ., 40, 65

66. Goncharovskiy, A.V., Ryabchikova, T.A., Stepanov, V.V., Khokhlova, V.L. & Yagola, A.G. Doppler-Zeeman mapping of chemical elements on surface of Ap stars. 1983, Astron. Rep., 60, 83

67. Ptitsin, D.A. & Ryabchikova, T.A. Chemical composition of B star HD 204754, suspected in metal deficit. 1986, Astron. Rep., 63(3), 526

68. Sturenburg, S. Abundance analysis of the l Bootis stars. 1993, A&A, 277, 139

69. Paunzen, E., Kamp, I., Iliev, I. Kh. et. all. Physical parameters of λ Bootis stars. 1999, A&A, 345, 597

70. Paunzen, E. & Maitzen, H.M. New variable chemically peculiar stars identified in the Hipparcos archive. 1998, A&AS, 133, 1

71. Romanyuk, I.I. Diagnostic technique of magnetic fields. 2005, Bull. Spec. Astrophys. Observ., 58, 64

72. Bohlender, D.A. & Landstreet, J.D. The abundance pattern of the l Bootis stars. 1990, MNRAS, 247, 606

73. Hunger, K. In: Upper Main Sequence CP stars. IAU Coll. 1986, Crimea, Reidel, 90, 257

74. Glagolevskii, Yu.V., Kopylova, F.G. On dependence of helium abundance upon magnetic field in He-r stars. 1991, Astrophys. Stud. (Bull. SAO), 34., 131

75. Khokhlova, V.L., Vasilchenko, D.V., Stepanov, V.V. & Romanyuk, I.I. Experiment of Doppler Zeeman mapping of surface of rapidly rotating magnetic CP star HD 37776. 2000, Astron. Rep., 26(3), 217

76. Thompson, I.B. & Landstreet, J.D. The extraordinary magnetic variation of the helium-strong star HD 37776 : a quadrupole field configuration. 1985, ApJ, 289, L9

77. Hunger, K. In Problems in Stellar Atmospheres and Envelopes ed. Bascheck. Kogl, Traving, 1975, Verlag, 57

78. Borra, E.F., Landstreet, J.D., Thompson, I.B. The magnetic field of helium weak B stars. 1983, ApJS, 53(1), 151

79. Romanyuk, I.I., Elkin, V.G., et. all. Doppler-Zeeman mapping of the rapidly rotation magnetic CP star HD 37776. 1999, Bull. Spec. Astrophys. Observ., 46, 92

BAŞ ARDICILLIQDA YERLƏŞƏN KİMYƏVİ PEKULYAR MAQNİT ULDUZLARI

S. H. Əliyev

N.Tusi adına Şamaxı Astrofizika Rəsədxanası,
Azərbaycan Milli Elmlər Akademiyası, Şamaxı rayonu, Azərbaycan

İşdə baş ardıcıllıqda yerləşən kimyəvi pekulyar (CP) ulduzların bir hissəsi olan maqnit ulduzlarına dair icmalın birinci hissəsi verilmişdir. Kimyəvi pekulyar ulduzları digərlərindən fərqləndirən əsas əlamətlər və onların təsnifatlarına dair məlumatlar təsvir edilir. Göstərilmişdir ki, CP ulduzları (məşhur) Preston tərəfindən aşağıda göstərilən təsnifata ayrılırlar; Am/Fm, λBoo, Ap/Bp, Hg- Mn, He-güclü (strong) və He-zəif (weak). CP ulduzlarının əksəriyətinin fırlanma periodu 0,5-100 gün təşkil edir, lakin uzun periodlu kicik qrup ulduzlarda vardır. Müxtəlif tipli kimyəvi pekulyar ulduz atmosferlərinin kimyəvi tərkibi məsələsinə də baxılmışdır. Kimyəvi anomallığı yarada bilən müxtəlif mexanizmlər araşdırılmış və onlardan selektiv diffuziya hipotezinə daha cox üstünlük verilmişdir.

Açar sözlər: Kimyəvi pekulyar ulduzlar – Maqnit sahəsi